

Ozone source apportionment during peak summer events over southwestern Europe

María Teresa Pay¹, Gotzon Gangoi², Marc Guevara¹, Sergey Napelenok³, Xavier Querol⁴, Oriol Jorba¹, Carlos Pérez García-Pando¹

¹Earth Sciences Department, Barcelona Supercomputing Center, BSC, c/Jordi Girona, 29, 08034 Barcelona, Spain

²Department of Chemical and Environmental Engineering, University of the Basque Country UPV/EHU, ETSI-Bilbao School of Engineering, Alda. de Urquijo s/n, E-48013 Bilbao, Spain.

³U.S. EPA, Research Triangle Park, NC, USA.

⁴Institute of Environmental Assessment and Water Research, IDAEA-CSIC, c/Jordi Girona, 18-26, 08034 Barcelona, Spain.

Correspondence to: María Teresa Pay (maria.pay@bsc.es)

Abstract. It is well established that in Europe, high O₃ concentrations are most pronounced in southern/Mediterranean countries due to the more favorable climatological conditions for its formation. However, the contribution of the different sources of precursors to O₃ formation within each country relative to the imported (regional and hemispheric) O₃ is poorly quantified. This lack of quantitative knowledge prevents local authorities from effectively designing plans that reduce the exceedances of the O₃ Target Value set by the European Air Quality Directive. O₃ source attribution is a challenge because the concentration at each location and time results not only from local biogenic and anthropogenic precursors, but also from the transport of O₃ and precursors from neighbouring regions, O₃ regional and hemispheric transport and stratospheric O₃ injections. The main goal of this study is to provide a first quantitative estimation of the contribution of the main anthropogenic activity sectors to peak O₃ events in Spain relative to the contribution of imported (regional and hemispheric) O₃. We also assess the potential of our source apportionment method to improve O₃ modelling. Our study applies and thoroughly evaluates a countrywide O₃ source apportionment method implemented in the CALIOPE air quality forecast system for Spain at high resolution (4 x 4 km²) over a 10-day period characterized by typical summer conditions in the Iberian Peninsula (IP). The method tags both O₃ and its gas precursor emissions from source sectors within one simulation and each tagged species is subject to the typical physical processes (advection, vertical mixing, deposition, emission and chemistry) as the actual conditions remain unperturbed. We quantify the individual contributions of the largest NO_x local sources to high O₃ concentrations compared to the contribution of imported O₃. We show for the first time that imported O₃ is the largest input to the ground-level O₃ concentration in the IP, accounting for 46% to 68 % of the daily mean O₃ concentration during exceedances of the European Target Value. The hourly imported O₃ increases during typical northwestern advections (70-90%, 60-80 µg/m³), and decreases during typical stagnant conditions (30-40%, 30-60 µg/m³) due to the local NO titration. During stagnant conditions, the local anthropogenic precursors control the O₃ peaks in areas downwind of the main urban and industrial regions (up to 40% in hourly peaks). We also show that ground-level O₃ concentrations are strongly affected by vertical mixing of O₃-rich layers present in the free troposphere, which result from local/regional layering and accumulation, and

continental/hemispheric transport. Indeed, vertical mixing largely explains the presence of imported O₃ at ground level in the IP. Our results demonstrate the need for detailed quantification of the local and remote contributions to high O₃ concentrations for local O₃ management, being the O₃ source apportionment an essential analysis prior to the design of O₃ mitigation plans in any non-attainment area. Achieving the European O₃ objectives in southern Europe requires not only *ad hoc* local actions but
5 also decided national and European-wide strategies.

1 Introduction

Tropospheric ozone (O₃) is an air pollutant of major public concern as it harms human health (WHO, 2013) and sensitive vegetation (Booker et al., 2009), and contributes to climate change (Jacob and Winner, 2009). O₃ is formed in the atmosphere through nonlinear photochemical reactions among carbon monoxide (CO), peroxy radicals generated by the photochemical
10 oxidation of volatile organic compounds (VOC), and nitrogen oxides (NO_x) (Crutzen, 1973). Therefore, meteorological stagnation, high temperature, and low precipitation enhance tropospheric O₃ formation (Demuzere et al., 2009; Otero et al., 2016). Atmospheric circulation also controls the short and long-range transport of O₃ affecting its lifetime in the atmosphere (Monks et al., 2015). For example, the transport of precursors emitted in urban and industrialized areas may cause O₃ production downwind (Holloway et al., 2003).

15 According to the European Environmental Agency (EEA) around 95-98% of the population in Europe during 2013-2015 were exposed to O₃ concentrations that exceeded the guidelines of the World Health Organization (WHO) (EEA, 2017). These guidelines establish a maximum daily 8-hour averaged (MDA8) O₃ concentration of 100 µg m⁻³ never to be exceeded. The European Air Quality Directive (2008/50/EC) is less restrictive as it sets an O₃ Target Value of 120 µg m⁻³ for the MDA8
20 concentration, which can be exceeded up to 25 days per calendar year averaged over three years.

Southern European countries around the Mediterranean Basin are particularly exposed to exceedances of the O₃ Target Value in summer due to the influence of frequent anticyclonic and clear-sky conditions that favour photochemical O₃ formation in the troposphere (EEA, 2017). In addition, its geographic location also makes the Basin a receptor of the long-range transport
25 of pollution from Europe, Asia and even North America (Lelieveld et al., 2002; Gerasopoulos, 2005). The importance of long-range transport on surface O₃ has been studied in the Mediterranean Basin, indicating that the emission sources within the Basin have a dominating influence on surface O₃, while remote sources are more important than local sources for O₃ mixing ratios at higher altitudes (Richards et al., 2013; Safieddine et al., 2014). Recent studies suggest that the upper O₃-rich air masses could increase the surface O₃ concentration in the Mediterranean Basin (Kalabokas et al., 2017; Querol et al., 2018). Further
30 detailed and quantitative studies on the mechanism linking upper O₃-rich layer with increases of the ground-level O₃ concentration in episodes need further clarification particularly regarding the contribution of O₃ transported at regional and hemispheric scales.

Several studies in the Iberian Peninsula (IP) have addressed the causes of O₃ episodes looking at the circulation of air masses (Millán, 2014, and references therein). In the Atlantic region, the blocking anticyclones over Western Europe favour the inter-regional transport of O₃ in the area and its accumulation for several days during the most severe episodes (Alonso et al., 2000; Gangoiti et al., 2002, 2006; Valdenebro et al., 2011; Saavedra et al., 2012; Monteiro et al., 2016). On the other hand, in the Mediterranean coast, the typical summer synoptic meteorological conditions with a lack of strong synoptic advection, combined with the orographic characteristics and the sea and land breezes, favour episodes where high levels of O₃ are accumulated by recirculation of air masses loaded with O₃ precursors (Millán et al., 1997 and 2000; Toll and Baldasano, 2000; Gangoiti et al., 2001; Pérez et al., 2004; Jiménez et al., 2006; Gonçalves et al., 2009; Millán, 2014, Querol et al., 2017; Querol et al., 2018). The coupling between synoptic and mesoscale processes governing the levels of O₃ in the Western Mediterranean Basin need further research in order to understand the O₃ intercontinental contribution. Furthermore, from our understanding there is a lack of research quantifying the contribution of the activity sources to the O₃ local formation during peak events in this region.

O₃ analyses in the Western Mediterranean Basin show that regional background O₃ levels have remained high without significant changes (EEA, 2016; EMEP-CCC, 2016; Querol et al., 2016). However, they have increased at traffic and urban background sites (EEA, 2016; Querol et al., 2016; Sicard et al., 2016; Saiz-Lopez et al., 2017). The reasons behind the urban O₃ upward trend are not clear yet due to the complex VOC-NO_x regime; part of the O₃ increase may have resulted from the reduction of NO emissions relative to NO₂ and therefore to a lower NO titration effect in VOC-limited situations. The most intense O₃ events in the last decade, measured by the number of exceedances of the O₃ Target Value are recorded over areas downwind of large urban and industrial hot spots (Monterio et al, 2012; Querol et al., 2016; EEA, 2016). Overall, the number of these type O₃ events occur in June-July and during summer heatwaves (i.e., 2003 and 2015).

According to the European Air Quality Directive, in zones exceeding the O₃ Target Value, Member States must develop plans to attain compliance by reducing the emission of O₃ precursors. Abatement of tropospheric O₃ concentration in the Western Mediterranean Basin has been insufficient so far (Querol et al., 2018). Effective planning requires an accurate quantitative knowledge of the sources of these precursors and their respective contributions to the exceedances of the O₃ Target Value (Querol et al., 2016; Borrego et al., 2015). However, source attribution of surface O₃ concentration remains a challenge, because the concentration at each location and time results not only from local biogenic and anthropogenic precursors, but also from the transport of O₃ and its precursors from neighbouring regions, O₃ hemispheric transport (UNECE, 2010), and stratospheric O₃ injections (Monks et al., 2015).

At present, there are no methods based on observations that distinguish the origin of O₃. Despite their inherent uncertainties, Chemical Transport Models (CTMs) allow apportioning the contribution of any source (by sector and/or region) to O₃

concentrations. The most widely used approach is the “brute force” method, which consists on running an ensemble of simulations zeroing out the sources one by one and then comparing them with a baseline simulation that accounts for all of the sources. Several O₃ source apportionment studies at European scale have applied the brute force method to quantify the contribution of one or two emission sectors. For example, road transport emissions with the EMEP model (Reis et al., 2000),
5 biogenic and anthropogenic emissions with the Polyphemus model (Sartelet et al. 2012), transport-related emissions including road transport, shipping, and aviation with the WRF-CMAQ model (TRANSPHORM, 2014), and ship emissions with CAMx (Aksoyuglu et al., 2016). Brute force is simple to implement, as it does not require additional coding in the CTM. However, as it quantifies the contribution of each source based on its absence, it does not reproduce actual atmospheric conditions, and therefore it is susceptible to inaccuracies in the prediction of O₃ peaks under non-linear regimes (Cohan and Napelenok, 2011).
10 Actually, brute force is not suitable to retrieve source contributions when the relationship between emissions and concentration is non-linear, but it is useful for analysing the concentration responses to emission abatement scenarios (Clappier et al., 2017).

Recently, CTMs include algorithms that tag multiple pollutants by source (region and/or sector) all the way through the pollutant’s lifetime, from emission to deposition. This integrated source apportionment approach has several advantages. First,
15 it allows identifying the main sources contributing to high O₃ levels under actual atmospheric conditions, which is a preliminary step towards designing refined and efficient emission abatement scenarios. Second, as we show below, it supports enhanced model evaluation and therefore potential model improvements by identifying problems in emission estimates (sectors or regions) or chemical boundary conditions. The Integrated Source Apportionment Method (ISAM) within the Community Multiscale Air Quality (CMAQ) model has shown promising results for O₃ tagging, exhibiting less noise in locations where
20 brute force results are demonstrably inaccurate (Kwok et al., 2013, 2015). Recent ISAM experiments have quantified that the contribution of traffic in the cities of Madrid and Barcelona to the daily O₃ peaks downwind of the urban areas is particularly significant (up to 80-100 µgm⁻³) (Valverde et al., 2016a). O₃ tagging methods are also included in other regional and global models applied over Europe (Karamchandani et al., 2017; Butler et al., 2018).

25 The integrated source apportionment tools combined with high-resolution emission and meteorological models can help unravelling the sources responsible for peak summer events of O₃ in the Western Mediterranean Basin. Quantifying the contribution of emission sources during acute O₃ episodes is a prerequisite for the design of future mitigation strategies in the region. In this framework, the main goal of this study is to provide a first quantitative estimation of the contribution of the main anthropogenic activity sectors compared to the imported concentration (regional and hemispheric) to peak O₃ events in
30 Spain. We also assess the potential of our source apportionment method to improve O₃ modelling. Our study applies for the first time a countrywide O₃ source apportionment at high resolution over the IP during the period between July 21st and 31st, 2012, which is representative of the typical summer synoptic conditions in the region. We use the CMAQ-ISAM within the CALIOPE air quality forecast system for Spain (www.bsc.es/caliope), which runs at a horizontal resolution of 4x4 km² over

the IP. The system is fed by the HERMESv2.0 emission model, which provides disaggregated emissions based on local information and state-of-the-art bottom-up approaches for the most polluting sectors.

The paper is organized as follows. In Section 2 we introduce the CALIOPE system, the set-up of ISAM and the HERMESv2.0 emission model for O₃ source apportionment studies, and the methodology used to quantify evaluate the model. In Section 3 we demonstrate the representativeness of the selected episode, we evaluate the model, and we provide an analysis of the source-sector contribution to the Spanish O₃ under the different synoptic patterns occurring during the study period. In Section 4, we discuss our findings, the regulatory implications, and future research.

2 Methodology

2.1 Air quality model

We used the CALIOPE air quality modelling system (www.bsc.es/caliope) to simulate the O₃ dynamics over the IP during the selected episode. CALIOPE is described elsewhere (Baldasano et al., 2008; Pay et al., 2014; Valverde et al., 2016a; and reference therein). The system consists of the HERMESv2.0 emission model (Guevara et al, 2013), the WRF-ARWv3.6 meteorological model (Skamarock and Klemp, 2008), the CMAQ v5.0.2 chemical transport model (Byun and Schere, 2006) and the BSC-DREAM8bv2 mineral dust model (Basart et al., 2012). CALIOPE first runs over Europe at 12-km resolution (12x12 km², named EU12 domain) and then over the IP at 4-km resolution (4x4 km², named IP4 domain) (Fig. S1). In the present work, the system is configured with 38 sigma layers up to 50 hPa, both for WRF and CMAQ. The planetary boundary layer is characterized with approximately 11 layers, where the bottom layer's depth is ~39 m. The EU12 domain uses meteorological initial and boundary conditions from the Final Analyses provided by the National Centers of Environmental Prediction (FNL/NCEP) at 0.5° by 0.5°. The first 12 h of each meteorological run are treated as cold start, and the next 23 h are provided to the chemical transport model. Boundary conditions for reactive gases and aerosols come from the global MOZART-4/GEOS-5 model at 1.9° by 2.5° (Emmons et al., 2010). CMAQ uses the CB05 gas-phase mechanism with active chlorine chemistry, an updated toluene mechanism (CB05TUCL; Whitten et al., 2010; Sarwar et al., 2012), and the sixth generation CMAQ aerosol mechanism including sea salt, aqueous/cloud chemistry and the ISORROPIA II thermodynamic equilibrium module (AERO6; Reff et al., 2009; Appel et al., 2013). Table S1 depicts the remaining CALIOPE configuration options.

For the IP4 domain, HERMESv2.0 estimates emissions for Spain with a temporal and spatial resolution of 1 h and up to 1 km by 1 km, according to the Selected Nomenclature for Air Pollution (SNAP), which are then aggregated to 4-km resolution (Guevara et al., 2013). HERMESv2.0 is suitable for source apportionment studies thanks to its level of detail in the calculation of the emission fluxes by source (Guevara et al., 2014). HERMESv2.0 is currently based on 2009 data, which is the closest year with updated information on local emission activities in HERMES at the time this work started. For neighbouring

countries and international shipping activities, HERMESv2.0 uses the annual gridded national emission inventory provided by the European Monitoring and Evaluation Programme (EMEP) disaggregated to 4-km resolution using a SNAP-sector-dependent spatial, temporal and speciation treatment (Ferreira et al., 2013).

5 HERMESv2.0 integrates the Model of Emissions of Gas and Aerosols from Nature (MEGANv2.0.4; Guenther et al., 2006) to estimate VOCs and NO_x emissions from vegetation, which play a major role on O₃ photochemistry, using temperature and solar radiation from the WRF model. Note that we configured MEGAN to compute VOC emissions from cultivated crops; the agriculture emission module in HERMESv2.0 estimates the VOC from manure management and field burning of agricultural residues. In this study, we have updated MEGANv2.0.4 with emission factors from MEGANv2.1
 10 (<http://lar.wsu.edu/megan/guides.html>). In Sect. 2 of the supplement, we provide a comparison with measurements from the DAURE campaign (Pandolfi et al., 2014) showing the reasonably good behaviour of our modelled isoprene.

Urban VOC emissions could be a relevant source of O₃. Over Spanish urban areas, HERMESv2.0 estimates VOC emissions from road transport and the use of solvents (Fig. 1) following bottom-up approaches (Guevara et al., 2013). However,
 15 uncertainties in the estimation of urban VOC emission inventories, as stated recently by several works (Pan et al., 2015; Liu et al., 2017; McDonald et al., 2018; Lewis, 2018) makes uncertain the urban VOC contribution to tropospheric O₃. In order to overcome this problem, continuous monitoring of urban VOC should be performed in Spanish cities, following the example of other regions in which O₃ is also a major problem such as Mexico City (Jaimes-Palomera et al., 2016). In addition, the use of formaldehyde satellite observations to constrain urban VOC emissions could be also pointed out as a future task to improve
 20 the representativeness of urban emission inventories (Zhu et al., 2014).

2.2 Ozone source apportionment method

We applied ISAM to quantify contributions from different SNAP categories to the surface O₃ over the IP. The ISAM O₃ tagging method is a mass balance technique that tags both O₃ and its gas precursor emissions (NO_x and VOC) from each source sector within one simulation (Kwok et al., 2013, 2015). Each tagged species undertakes typical physical processes (advection,
 25 vertical mixing, deposition, emission and chemistry) without perturbing the actual conditions. The O₃ rate of change for each tag in any grid cell is calculated as follows (Eq. 1):

$$\frac{dC_{tag}}{dt} = P_{tag} - D \frac{C_{tag}}{\sum_{tag} C}, \quad (1)$$

Where C_{tag} represents the O₃ concentration related to a tagged source of interest, P_{tag} is the chemical production rate of O₃
 30 formed by the precursors emitted for each tag, and D is the total chemical destruction rate of O₃ in this grid cell. Different ratios of NO_x/VOC cause the formation of O₃ in each grid cell, which is controlled either by NO_x- or VOC-limited conditions. ISAM uses the ratio H₂O₂/HNO₃ to determine whether O₃ is NO_x- or VOC-sensitive (above or below 0.35, respectively)

(Zhang et al., 2009). The bulk O_3 concentration in each model grid cell (P_{bulk}) is equal to the sum of O_3 tracers that were produced in either NO_x or VOC-sensitive conditions (Eq. 2),

$$P_{bulk} = \sum_{tag} P_{tag} = \sum_{tag} P_{tag}^N + \sum_{tag} P_{tag}^V, \quad (2)$$

5

where P_{tag}^N and P_{tag}^V are the O_3 produced under NO_x - and VOC-limited conditions, respectively according Eqs. 3 and 4:

$$P_{tag}^{N,new} = P_{tag}^{N,old} + P_{bulk}^{new} \frac{\sum_x NO_{x,tag}}{\sum_{tag} \sum_x NO_{x,tag}}, \quad (3)$$

$$P_{tag}^{V,new} = P_{tag}^{V,old} + P_{bulk}^{new} \frac{\sum_y VOC_{y,tag} \times MIR_y}{\sum_{tag} \sum_y VOC_{y,tag} \times MIR_y}, \quad (4)$$

10 $NO_{x,tag}$ and $VOC_{j,tag}$ are the concentrations of the x nitrogen and y VOC species in CB05 that participate in the photochemical O_3 formation for each source sector tag and grid cell. MIR_y is the maximum incremental reactivity factor of each y species of VOC emitted by each source sector tag, corresponding to the O_3 generating potential of each single VOC species (Carter, 1994).

15 2.3 Ozone tagged species

Table 1 summarizes the O_3 tagged sources in the present study and Fig. 1a depicts the HERMESv2.0's estimates of the contribution by each SNAP category to the total emissions of O_3 precursors in Spain. The largest NO_x sources are road transport (SNAP7; 42%), non-road transport (SNAP8; 19%), manufacturing industries (SNAP34; 16%), and energy production (SNAP1; 16%). VOC are dominated by biogenic sources (SNAP11; 70%) and to a lesser extent by the agricultural sector (SNAP10; 11%), solvent and other product uses (SNAP6; 9%) and road transport (SNAP7; <7%). The selected (tagged) SNAP categories in this study are the energy, industrial, road transport and non-road transport sectors (Fig. 1b), which account for the 92% of the total NO_x emissions in Spain. An additional tracer (OTHR) gathers the remaining emission categories that were not explicitly tracked (i.e., SNAP2, 5, 6, 9, 10 and 11).

25 In addition to the selected sources, we tracked the contributions of the chemical boundary conditions (BCON) and the initial conditions (ICON). BCON represents both the O_3 directly transported through the IP4 domain boundaries and the formation of O_3 resulting from precursors that are also transported through the boundaries. BCON O_3 comes from the EU12 parent domain, which includes the O_3 produced in Europe and the O_3 transported at global scale (both tropospheric and stratospheric O_3) provided by the MOZART-4/GEOS model (Fig. S1). Hereinafter, we name BCON O_3 as the imported O_3 to the IP4 domain. Tagging the O_3 initial allows quantifying the number of spin-up days to minimize the impact of model initialization.

For the present run, we required 6 days of spin-up to set the contribution of initial conditions to less than 1% of the net hourly O₃ concentration over 95% of the available O₃ stations.

2.4 Evaluation method

We evaluate the simulated concentrations against air quality measurements from the Spanish monitoring stations that are part of the European Environment Information and Observation Network (EIONET; <https://www.eionet.europa.eu/>). The EIONET network provides a relatively dense geographical coverage of the Spanish territory. During the July 21st-31st episode, we used the measurements from 347 stations for O₃ and 357 stations for NO₂ with a temporal coverage above 85% on an hourly basis. Fig. S2 shows the distribution of the stations for O₃ and NO₂.

The evaluation based on discrete statistics includes the correlation coefficient (r), Mean Bias (MB), Normalized Mean Bias (NMB) and the Root Mean Square Error (RMSE) (Appendix B). We used the package “openair” (Carslaw and Ropkins, 2012) for R (v3.3.2; R Core Team, 2016) to compute the statistics. We calculate statistics on an hourly basis for O₃ and NO₂, as well as for the regulatory MDA8 in the case of O₃. The evaluation also takes into account the station type, following the categories established by the EEA (i.e., rural background, suburban background, urban background, industrial and traffic).

There are no direct evaluation methods for apportioned pollutants. Instead, we designed a diagnostic plot for source apportionment analysis at each individual receptor, including a time series of measured and observed O₃ and NO₂ concentrations together with the simulated tagged sources. In addition, this plot includes the simulated wind speed and direction. These plots are helpful as they compare the modelled O₃ and NO₂ with the observations, while highlighting the sources and circulation patterns at least partly responsible for the model behaviour. This work will only discuss in detail the source apportionment plots at key O₃ receptor regions, given the high number of stations (260) that simultaneously measure O₃ and NO₂.

Evaluation results are discussed together with the source apportionment results. On the one side, the interpretation of the source apportionment results benefits from model evaluation. On the other side, the source apportionment results support enhanced model evaluation as it allows identifying potential errors in emission estimates for specific sectors and/or in the chemical boundary conditions.

3 Results

3.1 Description of the ozone episode

Our first estimation of the origin of peak O₃ events in Spain focuses on the episode July 21st -31st, 2012. Figure 2a illustrates the relevance of the episode showing the observed MDA8 O₃ concentrations trends at the Spanish EIONET stations during the (extended) summers (i.e., from April to September) from 2000 to 2012, together with the concentrations recorded during the episode. Although the selected episode is not the most severe between 2000 and 2012 at national scale, it comprises a period with high MDA8 O₃ concentrations measured at rural background stations, actually the 75th percentile of those values was above the Target Value, similar to the particularly severe summer of 2003 (Solberg et al., 2008).

This episode is also interesting because it was widespread and affected big parts of Europe (EEA, 2013). Only during this period 33% and 12% of the total number of exceedances for the information threshold and the Target Value in 2012, respectively, were measured. The O₃ regional context of the episode allows us to study the influence of the imported O₃ to Spain.

The maps of the 90th percentile of the measured MDA8 O₃ concentrations over Spain (Fig. 2b) show high concentration spots all over the domain. The exceedances of the Target Value were found in the surroundings of large urban areas (Madrid, Barcelona, Valencia, Seville) and along Spanish valleys (i.e., Ebro Valley, Guadalquivir Valley).

There were more than 100 exceedances of the O₃ Target Value in most of the days during the episode, with relative maxima on July 25th, 28th and 31st attributed to the change in the synoptic conditions (Fig. S3). Figure 3 shows the meteorological patterns (2m temperature, 10m wind, precipitation, mean sea level pressure and geopotential height at 500 hPa) modelled by WRF-ARW during the three distinctive days over the outer EU12 domain.

Our characterization of the study period is based on the circulation type classification proposed in Valverde et al. (2014), who developed an objective synoptic classification method over the period 1983–2012, specifically designed to study air quality dynamics over the IP. Stagnant conditions and northwestern advections are the most frequent summer synoptic circulation patterns over the IP, occurring ~44% of the days in a year (Jorba et al., 2004; Valverde et al., 2014). Stagnant conditions are characterized by reduced surface pressure gradients and weak synoptic winds, intense solar radiation, and the development of the Iberian Thermal Low (ITL). The ITL forces the convergence of surface winds from the coastal areas towards the central plateau enhancing sea breezes and mountain-valley winds and subsidence over the Western Mediterranean Basin as described by (Millán et al., 1997, 2000; Millán 2014). In contrast, northwestern advections (NWad) transport air masses from the Atlantic towards the north and west of the IP and they are characterized by atmospheric instability and intense ventilation. Periods of

accumulation and venting of pollutants follow the same sequence of pressure ridging and throughing respectively, of the lower and middle troposphere of the IP during the warm season (Querol et al., 2017; 2018). According to the circulation type classification in Valverde et al. (2014), the selected episode started with the development the ITL (July 21st-25th), followed by a NWad-venting period (July 26th-29th) and ended with the development of another ITL (July 30th-31st).

5

Figure 4 shows the 90th percentile (90p) of the simulated hourly O₃ and NO₂ concentrations corresponding to the three distinctive days with the relative maxima of exceedances. In the northern Spanish Mediterranean areas, intense O₃ episodes often affect the plains and valleys located 60 km north of the Barcelona Metropolitan Area (BMA) in summer (Toll and Baldasano, 2000; Gonçalves et al., 2009; Valverde et al., 2016a; Querol et al., 2017). High NO_x concentrations from the BMA combined with high biogenic VOC levels are driven inland by mesoscale processes (sea breezes and mountain-valley winds). This happened on July 31st when the highest 90p of the hourly O₃ concentrations (160-180 µgm⁻³) in Spain occurred over the north and northwest of the BMA. Occasionally, as it happened on July 25th, anticyclonic winds over the western Mediterranean Sea deflect the sea-breeze flow enriched with precursors from the BMA towards the Gulf of Lion where it reaches the highest 90p of the hourly O₃ concentrations (160-180 µgm⁻³) in the IP Mediterranean region. Eastern Spanish Mediterranean areas show similar O₃ dynamics, with inland regions depicting the highest O₃ peaks (140-160 µgm⁻³) when stagnant conditions cover central and eastern IP.

In the centre of the IP, intense O₃ episodes occurred during the development of the ITL, where the affected area depends on the synoptic conditions (Querol et al., 2018). Under the absence of synoptic forcing (e.g., July 25th), the MMA had the highest 90p of the hourly O₃ concentrations (~140-160 µgm⁻³). In contrast, when mountain valley winds are reinforced with synoptic westerlies (e.g., July 31st) (Fig. 3) the urban NO_x plume is channelled along the mountain ranges in Madrid towards the northeast and the highest 90p of the hourly O₃ concentrations are found along the valley (~140-160 µgm⁻³).

In the north and northeast of the IP, the 90p of the hourly O₃ concentrations show a significant increase when the blocking anticyclone over Western Europe is combined with the development of the ITL (e.g. July 25th). The stagnant conditions favour the accumulation of O₃ precursors around main cities and industrial areas and enhance the local O₃ formation.

The NWad pattern (e.g., July 28th) significantly decreases the 90p of the hourly O₃ concentrations in the centre and north of the IP. The northwesterly winds decrease the temperature and therefore the O₃ formation. As consequence, O₃ levels are reduced in the plumes from the BMA and the MMA, although they are still significant in the latter. Overall, the 90p of the hourly O₃ concentrations during the NWadv pattern were ~100 µgm⁻³ in most background areas. In contrast, during the ITL it was above 120 µgm⁻³.

3.2 Statistical evaluation

CALIOPE has been evaluated in detail elsewhere (Pay et al., 2014 and references therein). Furthermore, the system has been evaluated using the DELTA-Tool (Thunis and Cuvelier, 2014) developed by the Forum for Air Quality Modelling in Europe to support and harmonize the model evaluation in the frame of the Air Quality Directive. Valverde et al. (2015; 2016) used DELTA-Tool v4.0 and showed that CALIOPE accomplishes the quality objectives as defined in the Air Quality Directive for 78% of the NO₂ and 91% of the O₃ monitoring stations during the summer 2012. Here, we evaluate the updated version of CALIOPE using ISAM to quantify the system's ability to reproduce O₃ and NO₂ concentrations during the selected episode. Table 2 compiles the quartiles of the statistics calculated by station type.

The model slightly overestimates the average hourly and MDA8 O₃ concentrations with MB of +12 µgm⁻³ and +6 µgm⁻³, respectively. The *r* is above 0.6 in more than 50% of the stations and above 0.7 in 25% of them. The MB for average hourly and MDA8 O₃ concentrations are lower at RB stations (±4 µgm⁻³) than at IN, TR and UB stations (between +6 and +16 µgm⁻³) in 50% of the stations. As expected, the highest number of exceedances of the O₃ Target Value was recorded at RB stations (260 exceedances) followed by IN stations (204 exceedances).

At RB stations, average hourly O₃ is overestimated (+4 µgm⁻³) and MDA8 O₃ is underestimated (-4 µgm⁻³), which indicates that nighttime O₃ is overestimated. The nighttime overestimation is a common feature of CTMs and it is typically attributed to the underestimation of vertical mixing during nighttime stable conditions and to underestimation of the O₃ titration by NO (Bessagnet et al., 2016; Sharma et al., 2017).

CALIOPE underestimates the average hourly NO₂ concentrations with -7 µgm⁻³ at TR stations and -2 µgm⁻³ at RB stations. This partly explains the high overestimation of the average hourly and MDA8 O₃ concentration at TR and UB stations, as well as the systematic overestimation of average hourly O₃ concentration at nighttime (due to a lack of O₃ titration by NO). The average hourly NO₂ concentration at TR stations feature the highest *r* (with 25% of stations above 0.6), which proves the reasonably accurate representation of temporal emission in urban areas by the HERMESv2.0 (Guevara et al, 2014; Baldasano et al., 2011). In contrast, the RMSE is highest at TR stations, which results from the underestimation of NO₂ peaks during traffic rush hours. Underestimation of NO₂ traffic peaks is a common problem in Eulerian mesoscale models (Pay et al., 2014), as emission heterogeneity is lost in the grid cell-averaging process, which is especially critical in urban areas. Next generation microscale models will potentially solve this problem (Lateb et al., 2016). Besides the dilution of the emission in the grid, meteorology also may play an important role in the low performance of NO₂ and O₃ in hotspot areas. Several inter-comparison studies (e.g., EURODELTA and AQMEII) agree on the limitations of models to simulate meteorological variables that affect the average hourly NO₂ temporal variability, which controls model performance for O₃ in high NO_x environments and areas downwind (Bessagnet et al., 2016).

Figure 5 classifies the average hourly and MDA8 O₃ concentrations at the air quality stations into four MB categories that account for 93% of the stations. The best performances for O₃ (type B) are found at the 28% of the stations, located in the surroundings of the MMA, the BMA and most of the northern Mediterranean stations, which is consistent with the highest r ($0.6 < r < 0.9$) found in the centre and north of the IP (Fig. S4). The highest O₃ overestimations (type D) are present at 36% of the stations, mainly located in highly industrialized areas in Spain (Guadalquivir Valley, Strait of Gibraltar, Valencia) and inside the MMA. Next sections analyse the origin of these O₃ biases using the source apportionment time series.

The comparison with previous CALIOPE studies (Baldasano et al., 2011; Pay et al., 2014) indicates that r is in the same range for O₃ (0.6-0.7) and NO₂ (0.4-0.5) at individual stations; the same applies to the RMSE (15-29 µgO₃ m⁻³ and 10-20 µgNO₂ m⁻³). Modelled O₃ shows higher performance at traffic stations in large cities, since stations influenced by road transport emissions (i.e., high-NO_x environments) are better characterized with a more pronounced daily variability (Baldasano et al., 2011). At European scale, several model intercomparisons (Giornado et al. 2015; Bessagnet et al., 2016) indicate that O₃ concentrations in summer agree with the surface observations with r between 0.5 and 0.6. NO₂ hourly variability is overall underestimated due to uncertainties in the emission estimates, meteorological inputs and model resolution. These studies highlight the limitations of models to simulate meteorological variables that affect the NO₂ hourly variability, and therefore the model performance for O₃ in high-NO_x environments and downwind.

Section S4 in the supplement discusses the meteorological evaluation results and their impact on the pollutant concentrations. Not surprisingly, temperature shows the best behaviour when compared with observations (Table S2). The modelled wind speed is overestimated, particularly during nighttime (Fig. S5), coincident with low-level wind speed. The nighttime overestimation of wind is a source of error in modelled NO₂ and O₃ nighttime concentrations (Vautard et al., 2012; Bessagnet et al., 2016).

3.3 Source-sector ozone contributions during peak episodes

Figure 6 shows the 90p of the average hourly O₃ concentration over the IP tagged by source type (Table 1) for different days (July 25th, 28th and 31st). (Fig. S6 in the supplement shows similar plots for NO₂.) The imported O₃ is by far the largest contributor showing a 90p ranging from 70 to 120 µgm⁻³ in the east/north/centre of the IP on July 25th/28th/31st, respectively. The imported O₃ enters the study domain through the IP4 domain boundaries and it can only be transported, scavenged deposited or depleted by O₃ precursors. Therefore, areas with low imported O₃ concentrations (< 50 µgm⁻³) are good indicators of (1) the accumulation of specific O₃ precursors that deplete imported O₃, and (2) the subsequent O₃ photochemical production that occur mostly under stagnant conditions and around the largest industrial/urban areas. The 90p of the hourly imported O₃ concentration shows the lowest values in two different conditions and regions. On July 25th in the northwestern IP and Portugal, stagnant conditions allow the accumulation of pollutants that titrate imported O₃ concentrations down to 30-70 µgm⁻³. At the same time O₃ is locally produced due to traffic emission downwind of major northern cities (La Coruña, Gijón, Bilbao) (60-

120 μgm^{-3}), shipping activities (up to 40 μgm^{-3}) and the generation of energy and industrial processes (10-20 μgm^{-3}). On July 31st in the northeast of the IP, when the pollutants transported from the Gulf of Lion and Catalonia towards the Mediterranean act as a sink of imported O_3 reducing its concentration down to 60 μgm^{-3} . As a result, there is a local O_3 formation up to 120-160 μgm^{-3} along the Ebro Valley and the Lleida Plain. In a source attribution study over northern Portugal, Borrego et al. (2016) also found a reduction of imported O_3 and the subsequent O_3 formation by local sources under similar meteorological conditions.

After the imported O_3 , the largest contributor to O_3 is the road transport sector. Downwind of the major urban areas in Spain (i.e., Madrid, Barcelona, Bilbao, Seville, Valencia), on-road traffic contributed to the 90p of the hourly O_3 concentrations as much as 60-120 μgm^{-3} , and affected different areas depending on the synoptic/mesoscale regimes (Fig. 6). In the north of the BMA, the 90p of the hourly O_3 concentration from the road transport sector reaches its maximum when the stagnant conditions affects the centre and eastern IP (e.g., July 31st). As noted above, mesoscale winds carry traffic O_3 precursors from the BMA inland, channelled by north-south valleys towards the intra-mountain plain in the north. Over the MMA, the 90p of the hourly O_3 concentration from the road transport sector showed the maximum when the ITL was combined with the synoptic westerlies (e.g., July 31st), carrying high O_3 as far as to the Ebro Valley, as shown in Fig 4.

Regarding the contribution from the non-road transport sector, the Atlantic regions of the IP show the highest 90p of the average hourly O_3 concentration (25-40 μgm^{-3}) on July 25th. The stagnant condition favoured the accumulation of precursors from the Atlantic shipping route and the formation of O_3 within the region. The Spanish Mediterranean region shows the highest 90p of the average hourly O_3 concentrations from the non-road transport sector in front of the southeastern coasts of the IP (~180 μgm^{-3}) when the westerlies in the Strait of Gibraltar injected precursors from international shipping into the Mediterranean Basin (e.g., July 28th and 31st). Note that during days with high 90p of the average hourly O_3 concentration from non-road transport, the imported O_3 concentration shows the lowest 90p due to the NO titration effect over emission areas.

The elevated point source emission sectors (i.e., energy and industry) contributed less to O_3 than the traffic sector, but their contributions were significant reaching 15-25 μgm^{-3} of the 90p of the average hourly O_3 concentrations (Fig. 6). The north and northeast of the IP, the Mediterranean coast, and the Guadalquivir Valley are the most affected regions under stagnant conditions.

The contribution of the remaining sectors (OTHR) to the 90p of the average hourly O_3 concentrations was similar to that of the elevated point sources (15-25 μgm^{-3}), but it reached up to 30 μgm^{-3} in areas downwind of Oporto and Lisbon (Fig. 6). OTHR includes the formation of O_3 from the remaining anthropogenic and biogenic sources (accounting for less than 8% of total NO_x emissions, but 93% of total VOC). The high OTHR concentration around the biggest cities in Portugal may be

related to precursors emitted by the residential sector (SNAP2 and 9) and biogenic emissions, as found in other source apportionment studies over Portugal (Borrego et al., 2016; Karamchandani et al., 2017).

3.4 Regionalization of source-sector contributions

We have identified ten O₃ receptor regions with similar characteristics in terms of meteorological and geographical patterns, O₃ dynamics and main source contributors (Figs. 4 and 6). The receptor regions defined in our work are consistent with Diéguez et al. (2014) and Querol et al. (2016), who proposed a similar regionalization based on observations from air quality stations. Figure 7c shows the location of the air quality stations belonging to each receptor region corresponding to the centre of the IP (CIP), the east of the IP (EIP), the Ebro Valley (EV), the Guadalquivir Valley (GV), the Mediterranean Sea (MED), the northeast of the IP (NEIP), the north of the IP (NIP), the northwest of the IP (NWIP), the south of the IP (SIP) and the west of the IP (WIP).

Figure 7a shows the absolute O₃ contribution of each tagged source at air quality stations by region along with the modelled and observed daily mean concentration during exceedances of 120 µgm⁻³ of the observed MDA8 ozone. Note that differences between sectors are more evident when normalizing (Fig. 7b). (Table S3 compiles de numerical values of Fig. 7.) Fig. 7 indicates that during exceedances of the MDA8 target value there is a good agreement ($r = 0.79$) between the sum of apportioned O₃ and the observed concentrations over the receptor regions.

The MED region shows the highest imported O₃ contribution (76%) because it is relatively far away from important anthropogenic NO_x+VOC sources in the IP. Under the ITL influence (July 25th and 31st), MED received air masses enriched with on-road traffic precursors from southern France and the NEIP, which enhanced O₃ production up to 7%. Shipping emissions in the MED region contributed up to 8% of the total O₃.

After MED, there is a cluster of regions along the Spanish Mediterranean coast (i.e., NEIP, EV and EIP) showing imported O₃ contributions between 60 and 68 % of the daily mean O₃ under exceedances. This is explained by their proximity to the eastern boundary and the frequent mesoscale phenomena enhancing the recirculation and accumulation of imported O₃ along the Spanish Mediterranean coasts. The contribution of road and non-road transport is similar (~11-16%) because these regions have both important roads and maritime trade routes. Note that the SIP region, which is also located in the Spanish Mediterranean coast, shows a daily mean imported O₃ concentration lower than the regions along the Spanish Mediterranean coast (~57%) and the highest non-road transport contribution in Spain (19%). The main sink of imported O₃ are precursors resulting from dense shipping traffic through the Strait of Gibraltar, which have substantial impact in the O₃ production downwind (either in the Alboran Sea or the Gulf of Cadiz).

The regions including the largest metropolitan areas in Spain are the CIP (Madrid) and the NEIP (Barcelona). Both regions show an imported O₃ contribution of ~60% and a similar contribution from the road transport sector (18 and 16%, respectively). However, the NEIP shows a slightly higher contribution from non-road transport (13 vs 10%) due to the influence of international shipping near coastal areas.

5

The northern and northwestern regions of the IP (NIP and NWIP) had relatively lower imported O₃ contributions (56-59%). The contribution of non-road transport was ~10-12%, slightly lower than in the Mediterranean coast, and that of road transport was also significant (~14-15%). The contribution from the industrial sector was one of the highest in the country (~5%) probably related to the influence of the large industrial facilities located in several areas of the north of Spain. The contribution from the energy sector in the NWIP region was the highest in Spain (~5%) due to emissions from large coal-fired power plants located in the area.

10

The WIP had the lowest daily mean O₃ concentrations during days exceeding the O₃ Target Value (93.5 µg m⁻³) and a high imported O₃ contribution (~63%). NO_x emissions in the WIP region are moderate (Fig. 4), which could explain the low daily mean O₃ concentration. There is a significant contribution from traffic (14% for road transport and 11% for non-road transport) and industrial and energetic sectors (7%) to the daily mean O₃ concentrations. These anthropogenic contributions suggest that O₃ in the WIP may be produced by precursors transported from the surrounding cities (Porto, Lisbon and Madrid) and the highly industrialized areas in the NWIP and the NIP (Fig. 6).

15

20 The Guadalquivir Valley had the lowest imported O₃ contribution of the IP (~46%) and the highest daily O₃ concentration during days of exceedance. The on-road traffic was the highest anthropogenic contributor to O₃ (~18%) due to the emissions from three major cities (Seville, Huelva, and Cordoba). Although O₃ in Huelva may be overestimated (as discussed later), shipping is the second most important contributor to O₃ in the Guadalquivir Valley (~17%) probably link to the important fluvial transport along the river. (The Guadalquivir River is one of the most important routes for merchandise transport in Europe.) In fact, the non-road transport sector is the highest contributor (~17-19%) in southern Spain, both in the Guadalquivir Valley and the SIP, also due to the dense maritime routes across the Strait of Gibraltar.

25

The following sections analyse the source apportionment results at regions with a high on-road traffic contribution (i.e., CIP and NEIP) and a high contribution from industry and energy production (i.e., NWIP and Guadalquivir Valley).

30 3.4.1 The centre of the Iberian Peninsula

Figure 8 show the source apportionment time series of the average hourly O₃ and NO₂ concentrations at two stations, an urban station in Madrid (station 1 in Fig. 8a), and another one located in Guadalajara (station 2 in Fig. 8b), which is a medium size city affected by Madrid's urban plume. At the urban station, the model reproduces the O₃ traffic cycle ($r = 0.66$ and MB=22.5

5 μgm^{-3}) featuring the typical low O_3 concentrations ($< 40 \mu\text{gm}^{-3}$) in the early morning and in the afternoon due to O_3 titration (Fig. 8a). However, O_3 was overestimated (MB type D) during daytime peaks due to the overestimation of the NO_2 morning peaks during stagnant conditions, coincident with the highest road transport contribution for both pollutants. The results point towards a poor representation of the meteorological condition in the city during the stagnant conditions as shown in the meteorological evaluation (Sect. 4 in the supplement).

At the urban station downwind (Fig. 8b) modelled O_3 is positively biased (MB type B) due to the underestimation of NO_2 . Note that the uncertainty in NO_2 traffic emissions in medium size cities is larger than in the largest urban areas (i.e. Madrid, Barcelona) because data is generally unavailable and emissions are estimated based on population density (Baldasano et al., 2011).

The imported O_3 is the main contributor in both stations, but O_3 formation due to traffic increases significantly during peaks in both stations. The highest O_3 concentrations ($\sim 160 \mu\text{gm}^{-3}$) are modelled when westerly winds channelled along the Tajo valley carry the polluted air masses in a NE direction. These results in an O_3 contribution of $\sim 70 \mu\text{gm}^{-3}$ from the road transport sector in areas downwind (see wind vectors in Fig. 8b on July 28th and 31st). The O_3 contribution from the industrial sector (whose precursors could come from facilities in the south of the MMA, Fig. 4) reinforces the O_3 peaks up to $\sim 10 \mu\text{gm}^{-3}$, meanwhile the contribution from non-road transport increases systematically the background O_3 concentration by $\sim 15 \mu\text{gm}^{-3}$. The O_3 contribution from non-road transport in this region may arise mainly from the Madrid's airports and the agricultural machinery operating in the surrounding rural areas.

20

3.4.2 The northeast of the Iberian Peninsula

Figure 8c and 8d show the source apportionment time series at two stations in the NEIP, an urban station in Barcelona (station 3) and a remote rural area downwind (station 4). Not surprisingly, at the urban station, NO_2 levels of up to $100 \mu\text{gm}^{-3}$ affect O_3 concentrations by titration during traffic peaks. In contrast, the rural station downwind depicts a higher O_3 and lower NO_2 concentration than the urban station. Absolute O_3 biases in both stations are $\sim 10 \mu\text{gm}^{-3}$ (MB type B).

25

O_3 mostly results from import and from the NO titration effect due to local road transport and industrial sources (Fig. 8c). However, the O_3 diurnal cycle in the urban areas of the NEIP is less marked than in the CIP due to persistently high O_3 concentration at night ($\sim 60 \mu\text{gm}^{-3}$). The breezes and mountain-valley winds contribute to the accumulation and recirculation of pollutants in this region.

30

At the rural station, modelled O_3 peaks ($> 120 \mu\text{gm}^{-3}$) are in a good agreement with observations (Fig. 8d), which suggests that overall the model reproduces the main transport paths, photochemical processes, and relative contributions from different

sources. Imported O₃ is one of the main contributors to ground-level O₃ (from 40 to 100 µgm⁻³), but during peaks the on-road traffic contribution sharply increases up to 80 µgm⁻³.

The O₃ concentration from the road transport sector arriving at rural areas in the NEIP, mainly comes from the Barcelona and surroundings as a result of the afternoon sea breezes (see wind vectors in Fig. 8c and 8d). However, under specific meteorological patterns these winds also carry precursors from other cities located in the NW Mediterranean Basin. Other authors (Gangoiti et al., 2001) have hypothesized that high O₃ concentration in the Western Mediterranean Basin is influenced by transport from France via the Carcassonne gap. The present experiment cannot quantify the contribution of French cities to the O₃ concentration over the NEIP, but future studies could explicitly tag the emission from the French regions.

10 3.4.3 Guadalquivir Valley

We have selected two stations along the Guadalquivir Valley, one in the urban area of Seville (station 5 in Fig. 9a), and one in a rural coastal area (station 6 in Fig. 9b). The contribution of non-road transport is due the influence of one of the largest Spanish harbours. The contribution of the energy sector to the O₃ concentration is also noticed (e.g., July 25th). As expected, the urban station (Fig. 9a) shows a high NO₂ concentration dominated by on-road traffic. NO_x from traffic is the main sink of O₃ in the city and the model reproduces the titration effect in agreement with observations (e.g., July 28th-31st).

High O₃ overestimations (10-30 µgm⁻³) at both stations (Fig. 9a and b) were detected during July 25th-28th which corresponds to intense and persistent SW winds transporting air masses from the Atlantic Sea along the Guadalquivir Valley, as shown by the wind vectors in Fig. 9a and b. Although the model overestimates O₃ concentrations, it reproduces the temporal variability. Our results suggest that the non-road transport sector is a significant contributor along the Guadalquivir Valley during these days. The impact of shipping emission on O₃ in the Guadalquivir Valley region is mainly evidenced by the relative high NO_x from ship exhaust (Fig. S3). NO₂ time series at the coastal station (Fig. 9b) indicates that the model overestimates NO₂ concentrations in hours where the NO₂ contribution from non-road transport is the highest. The unrealistic NO₂ peaks from non-road transport suggest that shipping emissions are overestimated in the HERMESv2.0 model, which uses the EMEP gridded emission inventory at 50 km x 50 km horizontal resolution to estimate shipping emissions and spatially distributes them to the 4-km model domain using the marine routes reported by Wang et al. (2008).

A recent review on the state-of-the-art of marine traffic emissions (Russo et al., 2018) indicates that STEAM appears as the most reliable and detailed emissions inventory since it is based on Automatic Identification System data and specific vessel information, with a resolution of 2.5 x 2.5 km² (Jalkanen et al., 2016). A comparative analysis indicates that EMEP gridded inventories are overestimated, in particular over hotspots in the Mediterranean shipping routes, and underestimated in secondary routes. This factor, added to the 15% decrease of NO_x shipping emissions observed in Europe between 2009 (HERMESv2.0 base year) and 2012 (EMEP CEIP, 2019) can at least partly explain the discrepancies observed.

3.4.4 The northwest of the Iberian Peninsula

Figures 9c and 9d show the source apportionment time series at one urban (station 7) and one rural (station 8) background station in the NWIP. The urban station (Fig. 9c) located in Santiago de Compostela, a medium size city with ~100,000 inhabitants, shows a high NO₂ concentration with a dominant contribution from the road transport sector. Traffic NO₂ is the main sink of urban O₃ via titration. Because NO₂ is underestimated, especially during stagnant conditions (July 24th-27th), O₃ concentrations are overestimated (MB category C).

Despite the O₃ biases during stagnant conditions, the modelled O₃ concentration is in general agreement with observations at the rural background station (Fig. 9d). NO₂ is likely to be underestimated due to missing traffic emissions. As noted previously, traffic emissions are poorly constrained in small and medium size cities, due to a lack of detailed information. There is also additional uncertainty in the precursors emitted from the large coal power plants and industries in the region (Valverde et al., 2016b). Our study uses emissions for 2009, and it has been estimated that between 2009 and 2012 energy production in coal-fired power plants increased from 13.1% to 19.4% (UNESA, 2012). This implies an increase in NO_x emissions from the power industry sector of around 19.5% (EMEP CEIP, 2019).

The time series show that the model reproduces reasonably well the observed O₃ variability under different synoptic conditions. O₃ reaches the highest concentration (~100/150 µgm⁻³ in urban/rural areas) under stagnant conditions (July 24th-27th) when the contribution of anthropogenic sources from all activity sectors is the highest (60-70%). O₃ concentrations decrease down to ~70 µgm⁻³ under NW advective conditions (e.g., July 28th-30th) when the imported O₃ shows the highest contribution (80-90%). Saavedra et al. (2012) found that stationary anticyclones over the NWIP play an important role in the occurrence of high O₃ concentrations. Our results show that under these stagnant conditions O₃ concentrations are due largely to in situ production (photochemistry) from on-road traffic, shipping, power plants, and industry in almost the same proportion.

3.5 Imported ozone

Our results indicate that imported O₃ represents the highest contribution to ground-level O₃ concentration in southwestern Europe. Imported O₃ enters the IP4 domain through the boundaries; it includes the contribution of O₃ from the EU12 domain, which in turn includes the contribution of hemispheric O₃ from the MOZART-4 global model. The imported O₃ is as large as the background O₃ regionally produced within the IP. Note that the small biases at rural background stations obtained in the evaluation section indicate an overall high performance of the modelled background O₃ in the IP4 domain (Fig. S1). Given the important implications and robustness of these results, we further analyse this contribution below. In particular, we aim to understand its high contribution within the IP, even far from the model domain boundaries.

Figure 10 shows the vertical cross-sections at 6, 12, and 18 UTC for O₃ and NO₂ at a constant latitude (40.38° N) on July 25th, 28th and 30th. It helps to understand the vertical variability of both pollutants according to the PBL as schematized by Millán et al. (1996). The model predicts a pronounced O₃ vertical gradient above a height of 4 km above sea level (asl), showing that O₃ in the free troposphere is, to a large extent, imported to the IP4 domain (Safieddine et al., 2014). As expected, NO₂ mixing ratios show a negative gradient with altitude as it is mainly emitted at the surface. In the morning, the sun starts to heat up the ground, producing convective thermals and forcing the growth of the mixing layer. At noon, the mixing height reaches its maximum, being the highest in the CIP (2-4 km) and decreasing towards the coast (< 1 km) (Fig. 10). At the mixing layer top the O₃-enriched air aloft is entrained into the mixing layer, mixing with O₃ and other pollutants produced locally within the mixing layer. When the mixing height decreases, O₃ is left in the free troposphere forming high O₃ residual layers (Gangoiti et al., 2001) that contribute to the regional transport. Over the following days, these residual layers (composed of imported O₃ and local O₃ produced within the domain over previous days) can be entrained by fumigation into the mixing layer to reach the surface. This fumigation effect, previously described in the eastern USA (Zhang and Rao, 1999; Langford et al., 2015) and in the Western Mediterranean Basin (Kalabokas et al., 2017; Querol et al., 2018), leads to a rapid increase in O₃ concentrations at ground level. The accumulation and recirculation of air masses is intensified along the Eastern Mediterranean coast (Millán et al., 1996, 2000; Gangoiti et al., 2001; Querol et al., 2017) by the action of the breezes and mountain-valley winds. Furthermore, the small deposition velocity of O₃ over the sea and its high atmospheric lifetime in the free troposphere contributes to enrich the O₃ background concentration (c.a. several weeks, Monks et al., 2015; Seinfeld and Pandis, 2016).

The O₃ fumigation effect was particularly intense on July 30th-31st, when a high O₃ levels are found in the free troposphere compared to previous days (Fig. 10). The analysis of the O₃ concentration map with the imported O₃ contributions (Fig. 6) indicates that ground-based O₃ is neither advected nor titrated; therefore, it can only result from vertical mixing. The high O₃ mixing ratio in the free troposphere was mainly due to O₃ advection entering the Atlantic boundary driven by westerlies (Fig. 3). We hypothesize that two events may have contributed to the increase of the O₃ concentration by long-range transport. First, a low-pressure system in the British Islands on July 28th could have transported significant O₃ amounts from the stratosphere to the free troposphere (Fig. S7). Second, O₃ episodes generated in mid-July over the Eastern USA predicted by the MOZART-4 model could have contributed to an increase in the O₃ transported from N America to Europe by the action of the prevailing westerlies (Fig. S7) associated with cyclonic systems along the “warm conveyor belt” (Pausata, et al., 2012; Derwent et al., 2015).

4 Discussion and conclusions

Our study has provided a first estimation of the main sources responsible for high O₃ concentration in the Western Mediterranean Basin during the period July 21st -31st, 2012. We used the Integrated Source Apportionment Method (ISAM) within the CALIOPE system to estimate the contribution of the main anthropogenic activity sectors to peak O₃ events in Spain compared to the imported O₃. In addition, the use of ISAM has allowed an in-depth evaluation of the model.

The results demonstrate that the O₃ problem over the Western Mediterranean Basin is local, regional, and hemispheric. Long-range transport of O₃ from beyond the IP domain is the main contributor to the ground-level daily mean O₃ concentration (~45%) during peak episodes. The imported O₃ contribution ranges from 40% during O₃ peaks to 80% at night or during well-ventilated conditions. The absolute imported O₃ is higher in the northeast of the IP than in the central IP due to the recirculation and accumulation of pollutants along the Mediterranean. The high imported O₃ at the surface far away from the model boundaries is consistent with the high levels of O₃ in the free troposphere (resulting from local/regional layering and accumulation, and continental/hemispheric transport) along with intense vertical mixing during the day.

Our results support the European Commission (EC, 2004) in pointing out that the effectiveness of abatement strategies for achieving compliance with the European air quality standards in southern Europe might be compromised by the long-range transport of O₃. This is especially true in Mediterranean regions (i.e., NEIP, EV and EIP) where the contribution of imported O₃ is particularly dominant (60-68% of the daily mean O₃ concentration) as a result of the accumulation and recirculation of pollutants over the Mediterranean Basin. In those areas, if the long-range transport of O₃ is not reduced, the mean background level will not decrease making it more vulnerable to exceedances of the O₃ target values by enhanced local production under stagnant conditions.

During high O₃ events, the imported O₃ is added to the formation from local and regional anthropogenic sectors. The road transport is an important contributor to the O₃ concentration in rural areas downwind of the large cities in Spain. It contributed up to 16-18% of the daily mean O₃ concentration under exceedances of the target value for human health protection, and up to 70 µgm⁻³ on an hourly basis downwind of Barcelona and Madrid.

The non-road transport sector (including international shipping, airport and agricultural machinery) is as significant as road transport inland (10-19% of the daily mean O₃ concentration during the peaks). There is a high influence of international shipping (13%), affecting the coastal areas in the Mediterranean and the south of the IP (along the Strait of Gibraltar) with contributions of up to ~20 and ~30 µg/m³, respectively. Although the non-road transport contribution was found to be overestimated in coastal areas in the south of the IP in the present experiment, it cannot be neglected and actions controlling international shipping should be considered as important as those related with road transport especially in regions with big

harbours (e.g., Huelva and Barcelona). Dalsøren et al. (2010) indicated that annual O₃ concentration is increasing yearly in a range of 0.5-2.5 ppb in areas impacted by shipping activities. Recent studies indicate that shipping emissions are projected to increase significantly due to increases in transportation demand and traffic. As the Strait of Gibraltar is the only shipping route connecting the Atlantic Ocean with the Mediterranean Basin, the regulation of these emissions is key in order to control O₃ exceedances in Spain and the Mediterranean Basin. Shipping emissions can be regulated by each country within 400 km of coastlines, but policy-induced controls for offshore emissions are very dependent on the success of adopted and proposed regulations within the International Maritime Organization.

The energy and industrial sectors contribute ~6-11% of the daily mean O₃ concentration during the peaks and over all the receptor regions. As they are usually injected in high altitudes, their contribution extends way beyond their surroundings. The energy combustion sector (3%) and industrial and non-industrial combustion sectors (3%) have a mean contribution of 2-4 µgm⁻³, going up to 4-6 µgm⁻³ in NO_x-limited areas (i.e., the western IP). In highly industrialized regions (i.e., Guadalquivir Basin and northwestern IP), abatement strategies affecting all sectors at regional scale could contribute to decrease the local formation of O₃ as the regional/local anthropogenic contribution can be greater than 50% during several days.

In the Barcelona Metropolitan Area the contribution from energy and industrial sectors to the NO₂ concentrations can be in the same range than the contribution from road transport (~40-60%, Fig. 8c). In contrast, in areas downwind Barcelona the contribution from energy and industrial sectors to O₃ concentrations is relatively low compared with the contribution from road transport (Fig. 8d). The different contribution to O₃ concentration might be related to with the different reactivity of VOC for O₃ formation. Each VOC emission source emits a different mix of VOC, which makes a different contribution to photochemical ozone formation. For example, in the UK, Derwent et al. (2007) showed a higher photochemical O₃ creation potential for road transport emissions than for production processes and combustion. Future national policy actions to control the emissions of VOC should tackle the sources that contribute more to photochemical O₃ formation.

The remaining sectors (i.e., SNAP 2, 5, 6, 9, and 11, see Table 1), are the fourth main contributors to the daily mean O₃ concentration during the days exceeding the target value (~2-8%). Future work should tag the biogenic sources as an individual sector as it is the main contributor to VOC emissions in Spain (i.e., ~70% in 2009 according to HERMESv2.0 model).

The air quality and meteorological evaluation indicate that uncertainties in our model are in the same range as the most recent inter-comparison studies using state-of-the-art air quality models. In addition, our model evaluation together with the source apportionment results has allowed a better understanding of the origin of model errors related to emission estimates. Our methodological choice has been to use a detailed bottom-up emission inventory instead of a typical top-down regional emission inventory. Bottom-up emissions, estimated using source-specific emission factors and activity statistics, accurately characterise pollutant sources and allow obtaining more realistic results than the ones reported by top-down or regional

emission inventories. To understand the impact of the use of 2009 data to study year 2012, we revised the EMEP Centre on Emission Inventories and Projections (EMEP-CEIP), which collects and reviews the national emission inventories from Parties to the Convention on Long-range Transboundary Air Pollution. Between 2009 and 2012, total NO_x and NMVOC emissions in Spain decreased by -10.6% and -10.7%, respectively (EMEP CEIP, 2019). For NO_x, around 80% of this reduction is linked to a reduction of road transport emissions, whereas in the case of NMVOC ~50% of the reduction is due to a decrease in industrial emissions. For our modelling study, we consider these differences as small and acceptable, and not creating any major inconsistency. The difference of 10-15 % in emissions for certain precursors between 2009 and 2012 is within the typically larger ranges of uncertainty in emission inventories.

Another relevant and uncertain source of O₃ is the VOC emitted in urban areas. Future research works should be devoted to the continuous monitoring of urban VOC and take advantage of satellite observations to improve speciation and spatial variability of urban VOC emissions.

We have identified two sources of uncertainty in the estimation of the imported O₃. First, it depends on both the performance of the CALIOPE system over EU12, and on MOZART-4 at global scale. The small biases at rural background stations support an overall high performance baseline background O₃ in the IP4 domain (Fig. S1). Second, our set-up involves some uncertainty in the estimation of the imported contribution of O₃. In reality, there is a fraction of the imported O₃ that may have been generated within the IP4 domain before the period of simulation (including the spin-up). We have assumed that this fraction is negligible and future works should check to what extent this assumption is correct.

For regulatory applications, further source apportionment studies should target not only emissions from activity sectors, but also the source regions where the emission abatement strategies should be applied. In addition, future studies should preferentially cover multiple summer periods in order to improve representativeness. We note that our results cannot predict whether emission abatement will have either a positive or a negative effect in O₃ changes due to the non-linearity of the O₃ generation process. Subsequent source sensitivity analyses tailoring the identified main contribution sources could predict how O₃ will respond to reductions in precursor emissions, which are essential to define the most efficient O₃ abatement strategies in the Western Mediterranean Basin.

Overall, we find that the imported O₃ is the largest input to the ground-level O₃ concentration in the IP during the studied episode. However, during stagnant conditions, the emission from local anthropogenic activities in the IP control the O₃ peaks in areas downwind of the main urban and industrial regions. Furthermore, ground-level O₃ concentrations are strongly affected by vertical downward mixing of O₃-rich layers in the free troposphere, which result from local/regional layering and accumulation, and continental/hemispheric transport. The importance of both imported and local contributions to the O₃ peaks in the IP demonstrates the need for detailed quantification of both contributions to high O₃ concentrations for local O₃

management. Furthermore, the influence of local sources and topographical and meteorological conditions in the high O₃ concentration indicate the importance of designing O₃ abatement policies at local scale.

This work has quantified the local and imported contributions to O₃ during an episode in a particular area in southwestern Europe. In addition, we have provided a perspective about the potential use of source apportionment method for regulatory studies in non-attainment regions. Further O₃ source apportionment studies targeting other nonattainment regions in Europe are necessary prior to design local mitigation measures that complement national and European-wide abatement efforts.

Data availability

Air quality measurements are available at the EIONET database (<https://www.eea.europa.eu/data-and-maps/data/airbase-the-european-air-quality-database-7>). The CMAQ code is available at the <https://www.cmascenter.org/>. The WRF-ARW code is available at http://www2.mmm.ucar.edu/wrf/users/download/get_source.html. Download Mozart-4 outputs are available at <http://www.acd.ucar.edu/wrf-chem/mozart.shtml>. The program that generates CMAQ boundary conditions from MOZART-4 output is available at: <http://www.camx.com/getmedia/a0c2d710-6187-47bb-af3f-bd9b4a4d19bb/mozart2camx-12jul17.tgz>. The HERMESv2 outputs are available upon request. The modelled data in this study are available upon request from the corresponding author.

Appendix A

Table 1A shows the acronyms used in the text.

BCON	Chemical boundary conditions to IP4, also named as imported O ₃ contribution
BMA	Barcelona Metropolitan Area
CIP	Central Iberian Peninsula
CMAQ	Community Multiscale Air Quality model
EIP	Eastern Iberian Peninsula
EU12	European domain at 12-km horizontal resolution (12x12 km ²)
EV	Ebro Valley
GV	Guadalquivir Valley
IP	Iberian Peninsula
IP4	Iberian Peninsula domain at 4-km horizontal resolution (4x4 km ²)
ISAM	Integrated Source Apportionment Method
MDA8	Maximum daily 8-hour average concentration
MMA	Madrid Metropolitan Area
MED	Mediterranean Sea
NEIP	Northeast of the Iberian Peninsula
NIP	North of the Iberian Peninsula
NWIP	Northwest of the Iberian Peninsula
SIP	South of the Iberian Peninsula

SNAP1	Emission sector on combustion in energy
SNAP34	Emission sector on combustion and processes in industry
SNAP7	Emission sector on road transport, exhaust and non-exhaust
SNAP8	Emission sector on non-road transport (international shipping, airport and agricultural machinery)
WIP	West of the Iberian Peninsula
WRF	Weather Research and Forecasting Model

Appendix B

Definition of the discrete statistics used in the evaluation: correlation coefficient (r , Eq. B1), mean bias (MB, Eq. B2), normalized mean bias (NMB, Eq. B3) and root mean squared error (RMSE, Eq. B4). Where $C_m(x, t)$ and $C_o(x, t)$ are the
5 modelled and observed concentrations at a location (x) and time (t); N is the number of pairs of data. $\overline{C_m}$ and $\overline{C_o}$ are the modelled and observed mean concentrations over the whole period, respectively.

$$r = \frac{\sum_{i=1}^N (C_m(x, t) - \overline{C_m})(C_o(x, t) - \overline{C_o})}{\sqrt{\sum_{i=1}^N (C_m(x, t) - \overline{C_m})^2} \sqrt{\sum_{i=1}^N (C_o(x, t) - \overline{C_o})^2}} \quad (B1)$$

$$MB = \frac{1}{N} \sum_{i=1}^N (C_m(x, t) - C_o(x, t)) \quad (B2)$$

$$10 \quad NMB = \frac{\sum_{i=1}^N (C_m(x, t) - C_o(x, t))}{\sum_{i=1}^N (C_o(x, t))} \times 100 = \left(\frac{\overline{C_m}}{\overline{C_o}} - 1 \right) \times 100 \quad (B3)$$

$$RMSE = \frac{1}{N} \sqrt{\sum_{i=1}^N (C_m(x, t) - C_o(x, t))^2} \quad (B4)$$

Acknowledgments

This study has been supported by the Spanish Ministry of Economy and Competitiveness and FEDER funds under the project
15 PAISA (CGL2016-75725-R). This work was granted to access to the High Performance Computer resources of the “Red Española de Supercomputación” (AECT-2017-1-0008). The views expressed in this article are those of the authors and do not necessarily represent the views or policies of the U.S. Environmental Protection Agency. Carlos Pérez García-Pando acknowledges long-term support from the AXA Research Fund, as well as the support received through the Ramón y Cajal programme (grant RYC-2015-18690) of the Spanish Ministry of Economy and Competitiveness.

References

- Adame, J.A., Lozano, A., Bolívar, J.P., De la Morena, B.A., Contreras, J., and Godoy, F.: Behaviour, distribution and variability of surface ozone at an arid region in the south of Iberian Peninsula (Seville, Spain), *Chemosphere*, 70, 841-849, doi: 10.1016/j.chemosphere.2007.07.009, 2008.
- 5 Aksoyoglu, S., Baltensperger, U., and Prévôt, A. S. H.: Contribution of ship emissions to the concentration and deposition of air pollutants in Europe, *Atmos. Chem. Phys.*, 16, 1895–1906, doi:10.5194/acp-16-1895-2016, 2016.
- Appel, K. W., Pouliot, G. A., Simon, H., Sarwar, G., Pye, H. O. T., Napelenok, S. L., Akhtar, F., and Roselle, S. J.: Evaluation of dust and trace metal estimates from the Community Multiscale Air Quality (CMAQ) model version 5.0, *Geosci. Model Dev.*, 6, 883–899, doi:10.5194/gmd-6-883-2013, 2013.
- 10 Baldasano, J.M., Jiménez-Guerrero, P., Jorba, O., Pérez, C., López, E., Güereca, P., Martín, F., Vivanco, M.G., Palomino, I., Querol, X., Pandolfi, M., Sanz, M.J., Diéguez, J.J.: Caliope: an operational air quality forecasting system for the Iberian Peninsula, Balearic islands and Canary islands e first annual evaluation and ongoing developments. *Adv. Sci. Res.* 2, 89-98, 2008.
- Baldasano, J.M., Pay, M.T., Jorba, O., Gassó, S., and Jiménez-Guerrero, P.: An annual assessment of air quality with the
- 15 CALIOPE modeling system over Spain. *Sci Total Environ*, 409, 2163-2178, doi: 10.1016/j.scitotenv.2011.01.041, 2011.
- Basart, S., Pérez, C., Nickovic, S., Cuevas, E., and Baldasano, J.M.: Development and evaluation of the BSC-DREAM8b dust regional model over Northern Africa, the Mediterranean and the Middle East, *Tellus B* 64, 18539, doi: 10.3402/tellusb.v64i0.18539, 2012.
- Bessagnet, B., Pirovano, G., Mircea, M., Cuvelier, C., Aulinger, A., Calori, G., Ciarelli, G., Manders, A., Stern, R., Tsyro, S.,
- 20 Gar- cía Vivanco, M., Thunis, P., Pay, M.-T., Colette, A., Couvidat, F., Meleux, F., Rouïl, L., Ung, A., Aksoyoglu, S., Baldasano, J. M., Bieser, J., Briganti, G., Cappelletti, A., D’Isidoro, M., Fi- nardi, S., Kranenburg, R., Silibello, C., Carnevale, C., Aas, W., Dupont, J.-C., Fagerli, H., Gonzalez, L., Menut, L., Prévôt, A. S. H., Roberts, P., and White, L.: Presentation of the EURODELTA III intercomparison exercise – evaluation of the chemistry transport models’ performance on criteria pollutants and joint analysis with meteorology, *Atmos. Chem. Phys.*, 16, 12667–12701, doi:10.5194/acp-16-12667-2016,
- 25 2016.
- Booker, F. L., Muntifer, R., McGrath, M., Burkey, K., Decoteau, D., Fiscus, E., Manning, W., Krupa, S., Chappelka, A. and Grantz, D.: The ozone component of global change: potential effects on agricultural and horticultural plant yield, product quality and interactions with invasive species, *J. Integrative Plant Biol.*, 51, 337-351, doi: 10.1111/j.1744-7909.2008.00805.x, 2009.
- 30 Borrego, C., Monteiro, A., Martins, H., Ferreira, J., Fernandes, A.P., Rafael, S., Miranda, A.I., Guevara, M., and Baldasano, J.M.: Air quality plan for ozone: an urgent need for North Portugal, *Air Qual. Atmos. Health* 8, 352–366, doi: 10.1007/s11869-015-0352-5, 2015.

- Butler, T., Lupascu, A., Coates, J., and Zhu, S.: TOAST 1.0: Tropospheric Ozone Attribution of Sources with Tagging for CESM 1.2.2, *Geosci. Model Dev. Discuss.*, <https://doi.org/10.5194/gmd-2018-59>, in review, 2018.
- Byun, D.W., and Schere, K.L.: Review of the governing equations, computational algorithms and other components of the Models-3 Community Multiscale Air Quality (CMAQ) Modeling System, *Appl. Mech. Rev.*, 59, 51–77, doi: 10.1115/1.2128636, 2006.
- Carslaw, D. C., and Ropkins, K.: Openair—an R package for air quality data analysis. *Environ. Modell. Softw.*, 27, 52-61, doi: 10.1016/j.envsoft.2011.09.008, 2012.
- Carter, W.P.L.: Development of ozone reactivity scales for volatile organic compounds, *J. Air Waste Manage. Assoc.*, 45, 4438-4445, doi: 10.1080/1073161X.1994.10467290, 1994.
- Clappier, A., Belis, C. A., Pernigotti, D., and Thunis, P.: Source apportionment and sensitivity analysis: two methodologies with two different purposes, *Geosci. Model Dev.*, 10, 4245-4256, <https://doi.org/10.5194/gmd-10-4245-2017>, 2017.
- Crutzen, P., J.: Photochemical reactions initiated by an influencing ozone in the unpolluted troposphere. *Tellus*, 26, 47-57, doi: 10.1111/j.2153-3490.1974.tb01951.x, 1975.
- Dalsøren, S. B., Eide, M. S., Myhre, G., Endresen, O., Isaksen, I. S. A., and Fuglestad, J. S.: Impacts of the large increase in international ship traffic 2000–2007 on tropospheric ozone and methane, *Environ. Sci. Technol.*, 44, 2482–2489, doi: 10.1021/es902628e, 2010.
- Demuzere, M., Trigo, R. M., Vila-Guerau de Arellano, J. and van Lipzig, N. P. M.: The impact of weather and atmospheric circulation on O₃ and PM₁₀ levels at a rural mid-latitude site, *Atmos. Chem. Phys.* 9, 2695-2714, doi: 10.5194/acp-9-2695-2009, 2009.
- Derwent, R., Jenkin, M.E., Passant, N.R., and Pilling, M.J.: Photochemical ozone creation potentials (POCPs) for different emission sources of organic compounds under European conditions estimated with a Master Chemical Mechanism, *Atmos. Environ.*, 41, 2570-2579, doi:10.1016/j.atmosenv.2006.11.019, 2007.
- Derwent, R., Utembe, S.R., Jenkin, M.E., and Shallcross, D.E.: Tropospheric ozone production regions and the intercontinental origins of surface ozone over Europe. *Atmos. Environ.*, 112, 216-224, doi: 10.1016/j.atmosenv.2015.04.049, 2015.
- Diéguez, J.J., Calatayud, V., and Mantilla, E.: Informe final. Memoria Técnica Proyecto CONOZE (Contaminación por Ozono en España). 139 pp. [Available at: [http://www.mapama.gob.es/es/calidad-y-evaluacion-ambiental/temas/atmosfera-y-calidad-del-aire/Informe_t%C3%A9cnico_CONOZE\[1\].tcm7-330956.pdf](http://www.mapama.gob.es/es/calidad-y-evaluacion-ambiental/temas/atmosfera-y-calidad-del-aire/Informe_t%C3%A9cnico_CONOZE[1].tcm7-330956.pdf), last access 7 September 2017], 2014.
- Domínguez-López, D., Adame, J.A., Hernández-Ceballos, M.A., Vaca, F., De la Morena, B.A., and Bolívar, J.P.: *Environ. Monit. Assess.*, 186, 5337-5351, 2014.
- EC: European Commission Decision of 19 March 2004. Concerning guidance for implementation of Directive 2002/3/EC of the European Parliament and the Council relating to ozone in ambient air (2004/279/EC). *Official Journal of the European Union* L87/50 of 25.3.2004., 2004.
- Eder, B., Kang, D., Mathur, R., Yu, S., and Schere, K.: An operational evaluation of the Eta-CMAQ air quality forecast model, *Atmos. Environ.*, 40, 4894-4905, doi: 10.1016/j.atmosenv.2005.12.062, 2006.

- EEA: Air pollution by ozone across Europe during summer 2012, EEA Report No 3/2013.. 48 pp. doi: <http://dx.doi.org/10.2800/70933>, 2013.
- EEA: Air quality in Europe – 2017 report. EEA Report, No 13/2017. ISSN 978-92-9213-920-9, 2017.
- EMEP-CCC: Air pollution trends in the EMEP region between 1990 and 2012, EMEPCCC-Report 2016/1 (102 pp.,
5 http://icpvegetation.ceh.ac.uk/publications/documents/EMEP_Trends_Report_final_published.pdf), 2016.
- EMEP CEIP, 2019. Officially reported emission data. Available at: http://www.ceip.at/ms/ceip_home1/ceip_home/data_viewers/official_tableau/ (last access February 2019)
- Emmons, L. K., Walters, S., Hess, P. G., Lamarque, J. F., Pfister, G. G., Fillmore, D., and Orlando, J.: Description and evaluation of the Model for Ozone and Related chemical Tracers, version 4 (MOZART-4). *Geosci. Model Dev.*, 3(1), 43-67,
10 doi: 10.5194/gmd-3-43-2010, 2010.
- Escudero, M., Lozano, A., Hierro, J., del Valle, J., and Mantilla, E.: Urban influence on increasing ozone concentrations in a characteristic Mediterranean agglomeration, *Atmos. Environ.*, 99, 322-332, doi: 10.1016/j.atmosenv.2014.09.061, 2014.
- Ferreira, J., Guevara, M., Baldasano, J.M., Tchepel, O., Schaap, M., Miranda, A.I., and Borrego, C.: A comparative analysis of two highly spatially resolved atmospheric emission inventories that are available in Europe, *Atmos. Environ.*, 75, 43-57,
15 doi:10.1016/j.atmosenv.2013.03.052., 2013.
- Foley, K. M., Roselle, S. J., Appel, K. W., Bhawe, P. V., Pleim, J. E., Otte, T. L., and Nolte, C. G.: Incremental testing of the Community Multiscale Air Quality (CMAQ) modeling system version 4.7, *Geosci. Model Dev.*, 3(1), 205-226, doi:10.5194/gmd-3-205-2010, 2010.
- Fowler, D., Brunkreef, B., Fuzzi, S., Monks, P.S., Sutton, M.A., Brasseur, G.P., Friedrich, R., Passante, L.G., and Jimenez-Mingo, J.M.: Research Findings in support of the EU Air Quality Review. Publications office of the European Union, Luxembourg, 2013.
20
- Gangoiti, G., Millán, M.M., Salvador, R., and Mantilla, E.: Long-range transport and re-circulation of pollutants in the western Mediterranean during the project Regional Cycles of Air Pollution in the West-Central Mediterranean Area, *Atmos. Environ.* 35, 6267–6276, doi:10.1016/S1352-2310(01)00440-X, 2001.
- Gangoiti G., Alonso L., Navazo M., Albizuri A., Pérez-Landa G., Matabuena M., Valdenebro V., Maruri M., García J.A., and Millán M. M.: Regional transport of pollutants over de Bay of Biscay: analysis of an ozone episode under a blocking anticyclone in west-central Europe, *Atmos. Environ.*, 36, 1349-1361, doi: 10.1016/S1352-2310(01)00536-2, 2002.
25
- Gangoiti G., Albizuri A., Alonso L., Navazo M., Matabuena M., Valdenebro V., García J.A., and Millán M. M.: Sub-continental transport mechanisms and pathways during two ozone episodes in northern Spain, *Atmos. Chem. Phys.*, 6, 1469-1484, doi: 10.5194/acp-6-1469-2006, 2006.
30
- Gerasopoulos, E., Kouvarakis, G., Vrekoussis, M., Kanakidou, M., and Mihalopoulos, N.: Ozone variability in the marine boundary layer of the Eastern Mediterranean based on 7-year observations, *J. Geophys. Res.*, 110, D15309, doi:10.1029/2005JD005991, 2005.

- Giordano, L., Brunner, D., Flemming, J., et al.: Assessment of the MACC reanalysis and its influence as chemical boundary conditions for regional air quality modeling in AQMEII-2. *Atmos. Environ.*, 115, 371–388, doi: 10.1016/j.atmosenv.2015.02.034, 2015.
- Gonçalves, M., Jiménez-Guerrero, P., and Baldasano, J.M.: Contribution of atmospheric processes affecting the dynamics of
5 air pollution in South-Western Europe during a typical summertime photochemical episode, *Atmos. Chem. Phys.* 9, 849–864, doi: 10.5194/acp-9-849-2009, 2009.
- Guenther, A., Karl, T., Harley, P., Wiedinmyer, C., Palmer, P., and Geron, C.: Estimates of global terrestrial isoprene emissions using MEGAN (Model of Emissions of Gases and Aerosols from Nature), *Atmos. Chem. Phys.* 6, 3181–3210, doi: 10.5194/acp-6-3181-2006, 2006.
- 10 Guevara, M., Martínez, F., Arévalo, G., Gassó, S., and Baldasano, J.M.: An improved system for modelling Spanish emissions: HERMESv2.0, *Atmos. Environ.*, 81, 209–221, doi: 10.1016/j.atmosenv.2013.08.053, 2013.
- Guevara, M., Pay, M.T., Martínez, F., Soret, A., van der Gon, H.D., and Baldasano, J.M.: Inter-comparison between HERMESv2.0 and TNO-MACC-II emission data using the CALIOPE air quality system (Spain), *Atmos. Environ.* 98, 134–145, doi: 10.1016/j.atmosenv.2014.08.067, 2014.
- 15 Holloway, T., Fiore, A., and Galanter Hastings, M.: Intercontinental transport of air pollution: will emerging science lead to a new hemispheric treaty?, *Environ. Sci. Technol.* 37, 4535–42, doi: 10.1021/es034031g, 2003.
- Im, U., Bianconi, R., Solazzo, E., et al.: Evaluation of operational on-line-coupled regional air quality models over Europe and North America in the context of AQMEII phase 2. Part I: Ozone. *Atmos. Environ.*, 115, 404–420, doi: 10.1016/j.atmosenv.2014.09.042, 2015.
- 20 Jacob, D., and Winner, D.: Effect of climate change on air quality, *Atmos. Environ.*, 43, 51–63, doi: 10.1016/j.atmosenv.2008.09.051, 2009.
- Jaimes-Palomera, M., Retama, A., Elias-Castro, G., Neria-Hernández, A., Rivera-Hernández, O., and Velasco, E.: Non-methane hydrocarbons in the atmosphere of Mexico City: Results of the 2012 ozone-season campaign, *Atmos. Environ.*, 132, 258–275, <https://doi.org/10.1016/j.atmosenv.2016.02.047>, 2016
- 25 Jalkanen, J.-P., Johansson, L., and Kukkonen, J.: A comprehensive inventory of ship traffic exhaust emissions in the European sea areas in 2011, *Atmos. Chem. Phys.*, 16, 71–84, <https://doi.org/10.5194/acp-16-71-2016>, 2016.
- Jiménez, P., Lelieveld, J., Baldasano, J.M.: Multiscale modelling of air pollutants dynamics in the northwestern Mediterranean basing during a typical summertime episode. *J. Geophys. Res.*, 111, D18306, doi: 10.1029/2005JD006516, 2006.
- Jorba, O., Pérez, C., Rocadenbosch, F., Baldasano, J.M.: Cluster analysis of 4-Day Back Trajectories Arriving in the Barcelona
30 Area, Spain, from 1997 to 2002. *J. Appl. Meteorol.*, 43, 887–901, 2004.
- Kalabokas, P., Hjorth, J., Foret, G., Dufour, G., Eremenko, M., Siour, G., Cuesta, J., and Beekmann, M.: An investigation on the origin of regional springtime ozone episodes in the western Mediterranean, *Atmos. Chem. Phys.*, 17, 3905–3928, <https://doi.org/10.5194/acp-17-3905-2017>, 2017.

- Karamchandani, P., Long, Y., Pirovano, G., Balzarini, A., and Yarwood, G.: Source-sector contributions to European ozone and fine PM in 2010 using AQMEII modeling data. *Atmos. Chem., Phys.*, 17, 5643-5664, doi: 10.5194/acp-17-5643-2017, 2017.
- Kranenburg, R., Segers, A.J., Hendriks, C., and Schaap, M.: Source apportionment using LOTOS-EUROS: module description and evaluation, *Geosci. Model Dev.*, 6, 721-733, doi: 10.5194/gmd-6-721-2013, 2013.
- Kwok, R. H. F., Napelenok, S. L., and Baker, K. R.: Implementation and evaluation of PM 2.5 source contribution analysis in a photochemical model. *Atmos. Environ.*, 80, 398-407, doi: 10.1016/j.atmosenv.2013.08.017, 2013.
- Kwok, R.H.F., Baker, K.R., Napelenok, S.L., and Tonnesen, G.S.: Photochemical grid model implementation and application of VOC, NO_x, and O₃ source apportionment. *Geosci. Model Dev.* 8, 99–114, doi: 10.5194/gmd-8-99-2015, 2015.
- Lateb, M., Meroney, R.N., Yataghene, M., Fellouah, H., Saleh, F., and Boufadel, M.C.: On the use of numerical modelling for near-field pollutant dispersion in urban environments – A review, *Environ. Poll.*, 208, 271-283, doi: 10.1016/j.envpol.2015.07.039, 2016.
- Langford, A. O., Sen, C. J., Alvarez, R. J., Brioude, J., Cooper, O. R., Holloway, J. S., Lind, M. Y., Marchbanksa, R. D., Pierce, R. B., Sandberg, S. P., Weickmann, A. M., and Williams, E. J.: An Overview of the 2013 Las Vegas Ozone Study (LVOS): Impact of stratospheric intrusions and long-range transport on surface air quality, *Atmos. Environ.*, 109, 305–322, 2015.
- Lelieveld, J., Berresheim, H., Borrmann, S., Crutzen, P. J., Dentener, F. J., Fischer, H., Feichter, J., Flatau, P. J., Heland, J., Holzinger, R., Kormann, R., Lawrence, M. G., Levin, Z., Markowicz, K.M., Mihalopoulos, N., Minikin, A., Ramanathan, V., de Reus, M., Roelofs, G. J., Scheeren, H. A., Sciare, J., Schlager, H., Schultz, M., Siegmund, P., Steil, B., Stephanou, E. G., Stier, P., Traub, M., Warneke, C., Williams, J., and Ziereis, H.: Global air pollution crossroads over the Mediterranean, *Science*, 298, 794–799, 2002.
- Lewis, A. C.: The changing face of urban air pollution. *Science*, 359, 744-745. doi:10.1126/science.aar4925, 2018.
- Liu, H., Man, H., Cui, H., Wang, Y., Deng, F., Wang, Y., Yang, X., Xiao, Q., Zhang, Q., Ding, Y., and He, K.: An updated emission inventory of vehicular VOCs and IVOCs in China, *Atmos. Chem. Phys.*, 17, 12709-12724, <https://doi.org/10.5194/acp-17-12709-2017>, 2017
- McDonald, B. C., de Gouw, J. A., Gilman, J. B., Jathar, S. H., Akherati, A., Cappa, C. D., Jimenez, J. L., Lee-Taylor, J., Hayes, P. L., McKeen, S. A., Cui, Y. Y., Kim, S.-W., Gentner, D. R., Isaacman-VanWertz, G., Goldstein, A. H., Harley, R. A., Frost, G. J., Roberts, J. M., Ryerson, T. B., and Trainer, M.: Volatile chemical products emerging as largest petrochemical source of urban organic emissions, *Science (New York, N.Y.)*, 359, 760–764, 2018.
- Millán, M.M.: Regional processes and long range transport of air pollutants in Southern Europe. The experimental evidence. In: Angeletti, G. (Ed.), *Physico-chemical Behaviour of Atmospheric Pollutants: Proceedings of the Sixth European Symposium*. European Commission, Luxembourg, pp. 445–459, 1994.
- Millán, M.M., Salvador, R., Mantilla, E., and Artiñano, B.: Meteorology and photochemical air pollution in southern Europe: experimental results from EC research projects. *Atmos. Environ.*, 30, 1909-1924, doi: 10.1016/1352-2310(95)00220-0, 1996.

- Millán, M.M., Salvador, R., Mantilla, E., and Kallos, G.: Photooxidant dynamics in the Mediterranean basin in summer: results from European research projects, *J. Geophys. Res.*, 102, 8811–8823, doi: 10.1029/96JD03610, 1997.
- Millán, M.M., Mantilla, E., Salvador, R., Carratalá, A., Sanz, M.J., Alonso, L., Gangoi, G., and Navazo, M.: Ozone cycles in the western Mediterranean basin: interpretation of monitoring data in complex coastal terrain, *J. Appl. Meteorol.* 39, 487–508, doi: 10.1175/1520-0450(2000)039<0487:OCITWM>2.0.CO;2, 2000.
- 5 Millán, M.M.: Extreme hydrometeorological events and climate change predictions in Europe, *J. Hydrol.*, 518, 206–224, doi: 10.1016/j.jhydrol.2013.12.041, 2014.
- Monks, P. S., Archibald, A.T., Colette, A., Cooper, O., Coyle, M., Derwent, R., Fowler, D., Granier, C., Law, K.S., Mills, G.E., Stevenson, D.S., Tarasova, O., Thouret, V., von Schneidemesser, E., Sommariva, R., Wild, O., and Williams, M.L.: Tropospheric ozone and its precursors from the urban to the global scale from air quality to short-lived climate forcer, *Atmos. Chem. Phys.* 15, 8889–8973, doi: 10.5194/acp-15-8889-2015, 2015.
- 10 Monteiro, A., Gama, C., Cândido, M., Ribeiro, I., Carvalho, D., & Lopes, M.: Investigating ozone high levels and the role of sea breeze on its transport. *Atmos. Poll. Res.*, 7(2), 339–347, 2016.
- Otero, N., Sillmann, J., Schnell, J.L., Rust, H.W., and Butler, T.: Synoptic and meteorological drivers of extreme ozone concentration over Europe. *Environ., Res. Lett.*, 11, 024005, doi: 10.1088/1748-9326/11/2/024005, 2016.
- 15 Orru, H., Andersson, C., Ebi, K. L., Langner, J., Åström, C., and Forsberg, B.: Impact of climate change on ozone-related mortality and morbidity in Europe, *Eur. Respir. J.*, 41(2), 285–294, doi: 10.1183/09031936.00210411, 2013.
- Pausata, F.S.R., Pozzoli, L., Vignati, E., and Dentener, F.J.: North Atlantic Oscillation and tropospheric ozone variability in Europe: model analysis and measurements intercomparisons, *Atmos. Chem. Phys.*, 12, 6357–6376, doi: 10.5194/acp-12-6357-2012, 2012.
- 20 Pandolfi, M., Querol, X., Alastuey, A., Jimenez, J.L., Jorba, O., Day, D., Ortega, A., Cubison, M.J., Comerón, A., Sicard, M., Mohr, C., Prévot, A.S.H., Minguillón, M.C., Pey, J., Baldasano, J.M., Burkhardt, J.F., Seco, R., Peñuelas, J., van Drooge, B.L., Artiñano, B., Di Marco, C., Nemitz, E., Schallhart, S., Metzger, A., Hansel, A., Lorente, J., Ng, S., Jayne, J., Szidat, S.: Effects of sources and meteorology on particulate matter in the Western Mediterranean Basing: An overview of the DAURE campaign. *J. Geophys. Res. Atmos.*, 119, 4978–5010, 2014.
- 25 Pay, M.T., Martínez, F., Guevara, M., and Baldasano, J.M.: Air quality at kilometre scale grid over Spanish complex terrains. *Geosci. Model Dev.* 7, 1979–1999, doi: 10.5194/gmd-7-1979-2014, 2014.
- Pérez, C., Sicard, M., Jorba, O., Comerón, A., and Baldasano, J. M.: Summertime re-circulations of air pollutants over the north-eastern Iberian coast observed from systematic EARLINET lidar measurements in Barcelona. *Atmos. Environ.*, 38, 3983–4000, doi: 10.1016/j.atmosenv.2004.04.010, 2004.
- 30 Querol, X., Alastuey, A., Reche, C., Orto, A., Pallares, M., Reina, F., Dieguez, J.J., Mantilla, E., Mantilla, M., Alonso, L., Gangoi, G., and Millán, M.: On the origin of the highest ozone episodes in Spain, *Sci. Tot. Environ.*, 572, 379–389, doi: 10.1016/j.scitotenv.2016.07.193, 2016.

- Querol, X., Gangoiti, G., Mantilla, E., Alastuey, A., Minguillón, M.C., Amato, F., Reche, C., Viana, M., Moreno, T., karanasiou, A., Rivas, I., Pérez, N., Ripoll, A., Brines, M., Ealo, M., Pandolfi, M., Lee, H.-K., Eun, H.-R., Park, Y.-H., Escudero, M., Beddows, D., Harrison, R.H., Bertrand, A., Marchand, N., Lyasota, A., Codina, B., Olid, M., Udina, M., Jiménez-Esteve, B., Soler, R.M., Alonso, L., Millán-M., and Ahn, K.-Ho.: Phenomenology of high ozone episodes in NE Spain, *Atmos. Chem. Phys.*, 17, 2817–2838, doi: 10.5194/acp-17-2817-2017, 2017.
- Querol, X., Alastuey, A., Gangoiti, G., Perez, N., Lee, H. K., Eun, H. R., Park, Y., Mantilla, E., Escudero, M., Titos, G., Alonso, L., Temime-Roussel, B., Marchand, N., Moreta, J. R., Revuelta, M. A., Salvador, P., Artíñano, B., García dos Santos, S., Anguas, M., Notario, A., Saiz-Lopez, A., Harrison, R. M., Millán, M., and Ahn, K.-H.: Phenomenology of summer ozone episodes over the Madrid Metropolitan Area, central Spain, *Atmos. Chem. Phys.*, 18, 6511–6533, <https://doi.org/10.5194/acp-18-6511-2018>, 2018.
- R Core Team: R: A language and environment for statistical computing. R Foundation for Statistical Computing, Vienna, Austria. Available at: <http://www.R-project.org/>, 2015.
- Reis, S., Simpson, D., Friedrich, R., Jonson, J. E., Unger, S., and Obermeier, A.: Road traffic emissions – predictions of future contributions to regional ozone levels in Europe, *Atmos. Environ.*, 34, 4701–4710, doi: 10.1016/S1352-2310(00)00202-8, 2000.
- Reff, A., Bhawe, P. V., Simon, H., Pace, T. G., Pouliot, G. A., Mobley, J. D., and Houyoux, M.: Emissions inventory of PM_{2.5} trace elements across the United States, *Environ. Sci. Technol.*, 43, 5790–5796, doi:10.1021/es802930x, 2009.
- Richards, N. A. D., Arnold, S. R., Chipperfield, M. P., Miles, G., Rap, A., Siddans, R., Monks, S. A., and Hollaway, M. J.: The Mediterranean summertime ozone maximum: global emission sensitivities and radiative impacts, *Atmos. Chem. Phys.*, 13, 2331–2345, doi:10.5194/acp-13-2331-2013, 2013.
- Russo, M. A., Leitão, J., Gama, C., Ferreira, J., & Monteiro, A.: Shipping emissions over Europe: A state-of-the-art and comparative analysis. *Atmospheric Environment*, 177, 187–194, 2018.
- Saavedra, S., Rodríguez, A., Taboada, J. J., Souto, J. A., and Casares, J. J.: Synoptic patterns and air mass transport during ozone episodes in northwestern Iberia. *Sci. Tot. Environ.*, 441, 97–110, doi: 10.1016/j.scitotenv.2012.09.014, 2012.
- Safieddine, S., Boynard, A., Coheur, P.-F., Hurtmans, D., Pfister, G., Quennehen, B., Thomas, J. L., Raut, J.-C., Law, K. S., Klimont, Z., Hadji-Lazaro, J., George, M., and Clerbaux, C.: Summertime tropospheric ozone assessment over the Mediterranean region using the thermal infrared IASI/MetOp sounder and the WRF-Chem model, *Atmos. Chem. Phys.*, 14, 10119–10131, doi:10.5194/acp-14-10119-2014, 2014.
- Saiz-Lopez, A., Borge, R., Notario, A., Adame, J.A., de la Paz, D., Querol, X., Artíñano, B., Gómez-Moreno, F.J., and Cuevas, C.A.: Unexpected increase in the oxidation capacity of the urban atmosphere of Madrid, Spain, *Sci. Rep.*, 7, 45956, doi: 10.1038/srep45956, 2017.
- Sarwar, G., Simon, H., Bhawe, P., and Yarwood, G.: Examining the impact of heterogeneous nitryl chloride production on air quality across the United States, *Atmos. Chem. Phys.*, 12, 6455–6473, doi:10.5194/acp-12-6455-2012, 2012.

- Sartelet, K. N., Couvidat, F., Seigneur, C., and Roustan, Y., 2012. Impact of biogenic emissions on air quality over Europe and North America, *Atmos. Environ.*, 53, 131–141, doi: 10.1016/j.atmosenv.2011.10.046, 2012.
- Seinfeld, J. H., Pandis, S. N.: *Atmospheric chemistry and physics: from air pollution to climate change*. John Wiley & Sons, 2016.
- 5 Sharma, S., Sharma, P., and Khare, M.: Photo-chemical transport modelling of tropospheric ozone: a review, *Atmos. Environ.*, 159, 34–54, doi: 10.1016/j.atmosenv.2017.03.047, 2017.
- Sicard, P., Serra, R., and Rossello, P.: Spatiotemporal trends in ground-level ozone concentrations and metrics in France over the time period 1999–2012, *Environ. Res.*, 149, 122–144, doi: 10.1016/j.envres.2016.05.014, 2016.
- Skamarock, W.C., and Klemp, J.B.: A time-split nonhydrostatic atmospheric model for weather research and forecasting applications, *J. Comput. Phys.* 227, 3465–3485, doi: 10.1016/j.jcp.2007.01.037, 2008.
- 10 TRANSPHORM: Source Contributions of Transport Emissions for European Air Quality and Exposure, Deliverable 2.4.4, available at: <http://www.transphorm.eu/Portals/51/Documents/Deliverables/New%20Deliverables/D2.4.4%20Source%20contributions%20of%20transport%20emissions%20for%20European%20air%20quality%20and%20exposure.pdf> (last access: 11 August
- 15 2017), 2014.
- Solberg, S., Hov, Ø., Søvde, A., Isaksen, I.S.A., Coddeville, P., De Backer, H., Foster, C., Orsolini, Y., and Uhse, K.: European surface ozone in the extreme summer 2003. *J. Geophys. Res.*, 113, D07307, doi:10.1029/2007JD009098, 2008.
- UNECE: Hemispheric transport of air pollution 2010. Part A: ozone and particulate matter. *Air Pollution Studies*, 17. UNECE, LRTAP, Task Force on Hemispheric Transport of Pollutants HTAP 2010: Part A. Ozone and Particulate Matter (278 pp,
- 20 ECE/EB.AIR/100, ISBN 978–92–1–117043–6,), 2010.
- Thunis, P., Cuvelier, C., 2014. DELTA Version 4.0. Joint Research Center, Ispra (http://aqm.jrc.ec.europa.eu/DELTA/assessment/data/DELTA_UserGuide_V4_0.pdf).
- Soret, A., Guevara, M., Baldasano, J.M., 2014. The potential impacts of electric vehicles on air quality in the urban areas of Barcelona and Madrid (Spain). *Atmospheric Environment*, 99, 51–63.
- 25 UNESA: Spanish Electricity Industry Association. Electricity Statistical Report 2012. Available at: <http://www.unesa.es/biblioteca/category/10-memorias>, 2012.
- Valdenebro, V., Gangoiti, G., Albizuri, A., Alonso, L., Navazo, M., García, J.A., Iza, J., and Millán, M.M.: Build-up and decay of two ozone episodes through northern Iberia and southern France – An inter-regional transport analysis, *Atmos. Environ.*, 45, 1591–1603, doi: 10.1016/j.atmosenv.2010.12.031, 2011.
- 30 Valverde, V., Pay, M.T., and Baldasano, J.M.: Circulation-type classification derived on a climatic basis to study air quality dynamics over the Iberian Peninsula, *Int. J. Climatol.* 35 (8), doi: 10.1002/joc.4179, 2014.
- Valverde, V., Pay, M.T., and Baldasano, J.M.: Ozone attributed to Madrid and Barcelona on-road transport emissions: characterization of plume dynamics over the Iberian Peninsula, *Sci. Total Environ.* 543, 670–682, doi: 10.1016/j.scitotenv.2015.11.070, 2016a.

- Valverde, V., Pay, M.T., and Baldasano, J.M.: A model-based analysis of SO and NO dynamics from coal-fired power plants under representative synoptic circulation types over the Iberian Peninsula, *Sci. Total Environ.*, 541, 701-713, doi: 10.1016/j.scitotenv.2015.09.111, 2016b.
- Vautard, R., Moran, M. D., Solazzo, E., Gilliam, R. C., Matthias, V., Bianconi, R., Chemel, C, Ferreira, J., Geyer, B., Hansen, A.B., Jericevic, A., Prank, M., Segers, A., Silver, J.D., Werhahn, J., Wolke, R., Rao, S.T., and Galmarini, S.: Evaluation of the meteorological forcing used for the Air Quality Model Evaluation International Initiative (AQMEII) air quality simulations. *Atmos. Environ.*, 53, 15-37, 2012.
- Wagstrom, K.M., Pandis, S.N., Yarwood, G., Wilson, G.M., and Morris, R.E.: Development and application of a computationally efficient particulate matter apportionment algorithm in a three dimensional chemical transport model, *Atmos. Environ.*, 42, 5650-5659, doi: 10.1016/j.atmosenv.2008.03.012, 2008.
- Wang, C., Corbett, J.J., Firestone, J.: Improving Spatial Representation of Global Ship Emissions Inventories, *Environ. Sci. Technol.*, 42, 193-199, doi: 10.1021/es0700799, 2008.
- WHO: Review of evidence on health aspects of air pollution - REVIHAAP project: technical report. WHO Regional Office for Europe, Copenhagen (302 pp., http://www.euro.who.int/_data/assets/pdf_file/0004/193108/REVIHAAP-Final-technical-report-final-version.pdf?ua=1), 2013.
- Whitten, G. Z., Heo, G., Kimura, Y., McDonald-Buller, E., Allen, D. T., Carter, W. P. L., and Yarwood, G.: A new condensed toluene mechanism for Carbon Bond: CB05-TU, *Atmos. Environ.*, 44, 5346–5355, doi: 10.1016/j.atmosenv.2009.12.029, 2010.
- Zhang, J., and Rao, S.T.: The role of vertical mixing in the temporal evolution of ground-level ozone concentration. *J. Appl. Meteorol.*, 38, 1674-1690, doi: 10.1175/1520-0450(1999)038<1674:TROVMI>2.0.CO;2, 1999.
- Zhang, Y., Wen, X-Y., Wang, K., Vijayaraghavan, K., and Jacobson, M.S.: Probing into regional O₃ and particulate matter pollution in the United States: 2. An examination of formation mechanisms through a process analysis technique and sensitivity study, *J. Geos. Res.*, 114, D22305, doi: 10.1029/2009JD011900, 2009
- Zhu, L., Jacob, D. J., Mickley, L. J., Marais, E. A., Cohan, D. S., Yoshida, Y., Duncan, B. N., González Abad, G., and Chance, K. V.: Anthropogenic emissions of highly reactive volatile organic compounds in eastern Texas inferred from oversampling of satellite (OMI) measurements of HCHO columns, *Environ. Res. Lett.*, 9, 114004, doi:10.1088/1748-9326/9/11/114004, 2014.

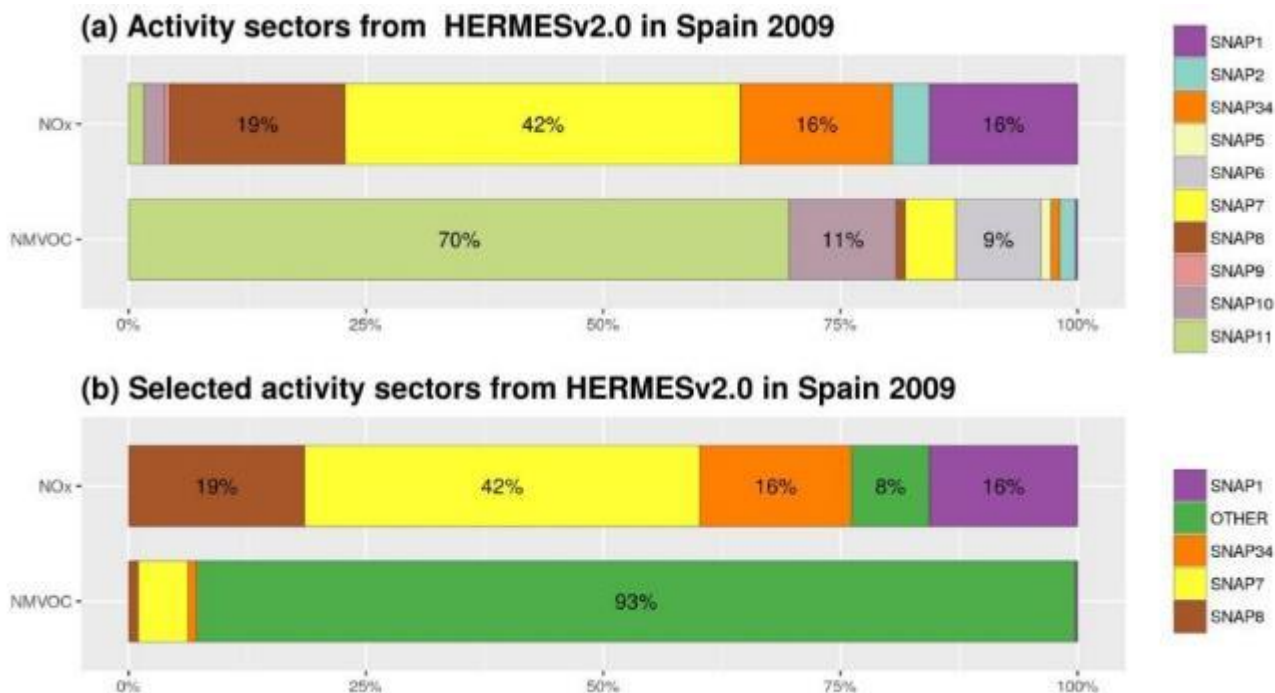


Figure 1: Percentage of the contribution of emissions to total annual emissions by SNAP sector calculated by HERMES for Spain 2009 (a) and for the selected SNAP sector accounting for more than 90% of NO_x total emission to be tracked with ISAM (b). “OTHER” compiles the SNAP categories 2 (Residential combustion), 5 (Fugitive emissions from fuels), 6 (Solvent use), 9 (Waste management), 10 (Agriculture) and 11 (Other sources).

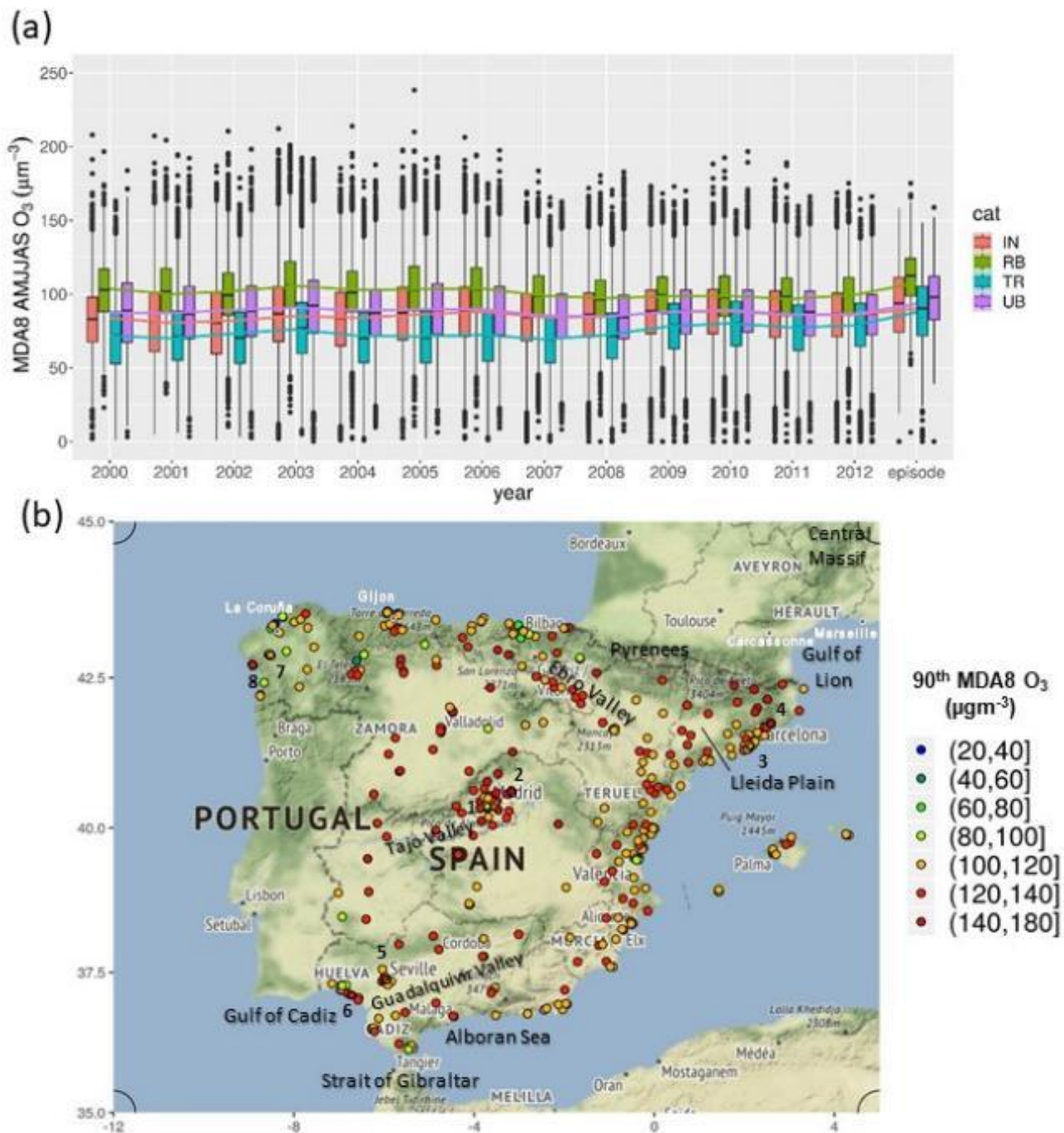


Figure 2: (a) Temporal distribution of the MDA8 O₃ concentration during the extended summer (from April to September, AMJJAS) at the Spanish EIONET stations for the period 2000-2012 and the episode (from 21/07/2012 to 31/07/2012) by

station type: IN (industrial), RB (rural background), TR (traffic) and UB (urban background). (b) 90th percentile of the MDA8 O₃ concentration at the Spanish EIONET stations during the episode. Numbers indicate the stations cited in section 3.4.

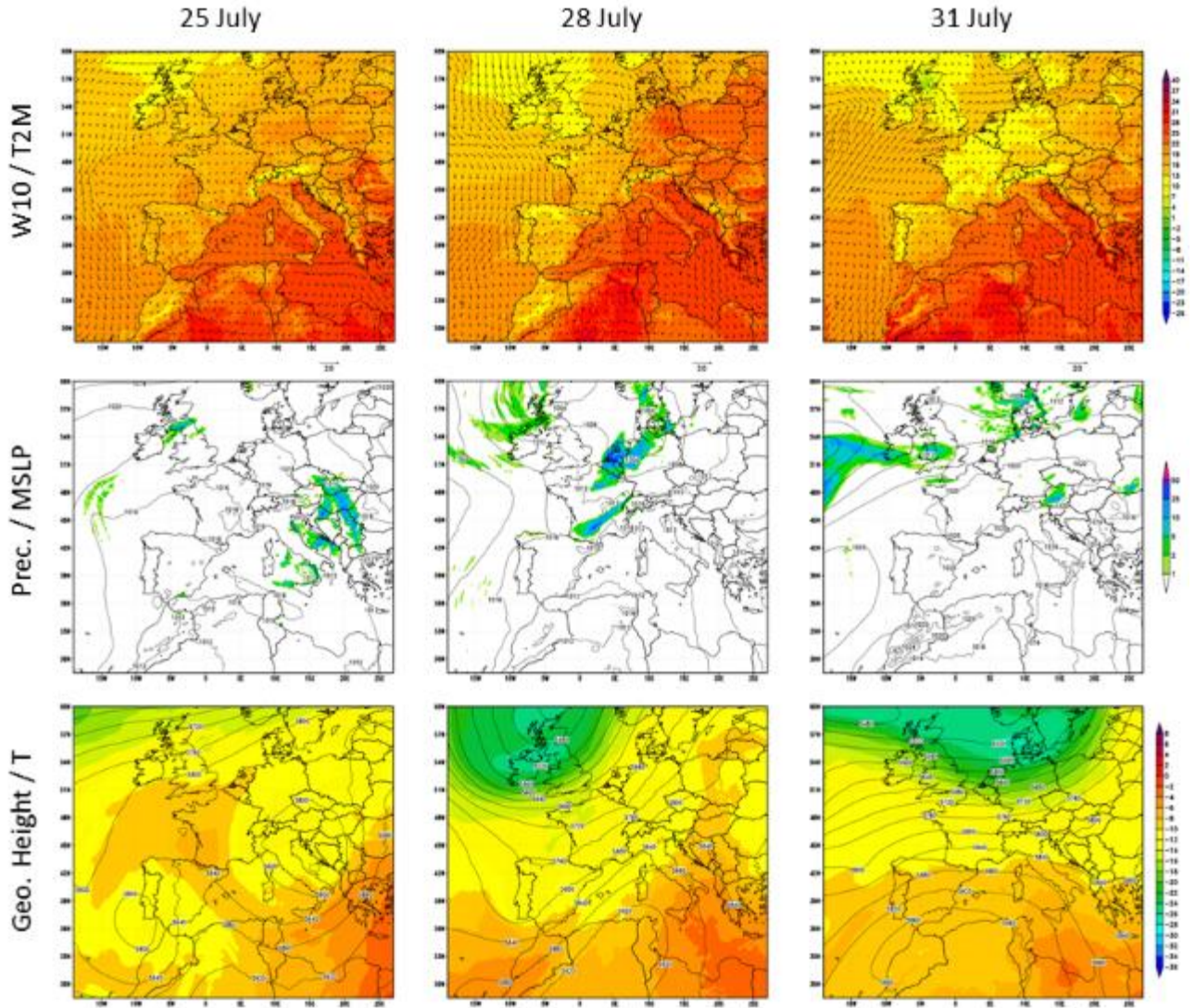


Figure 3: WRF-ARW meteorological fields at 6 UTC for July 25th, 28th and 31st in the EU12 domain: 10-m wind speed (W10, ms⁻¹), 2-m temperature (T2M, C), 6 h accumulated precipitation (Prec., mm), mean sea level pressure (MSLP, hPa), 500-hPa geopotential height in contours (Geo. Height, m), and 500-hPa temperature in shaded colors (T, °C).

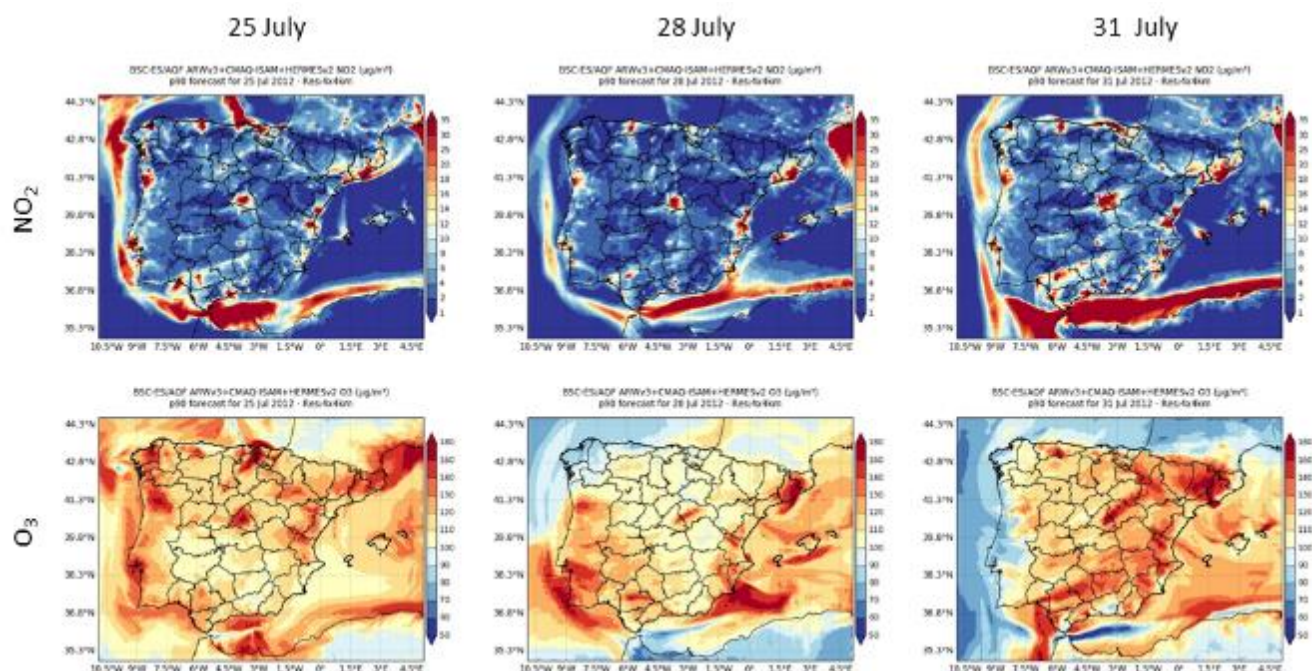
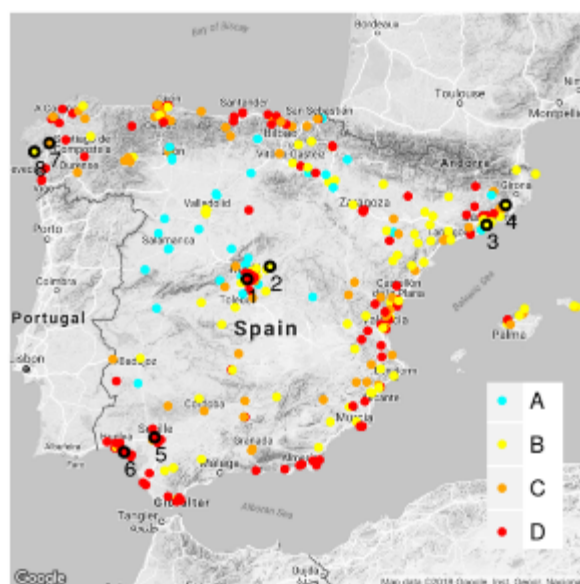


Figure 4: Ground-based concentration maps (in $\mu\text{g}/\text{m}^3$) for NO_2 (first row) and O_3 (second row) corresponding to the 90th percentile of the average hourly concentrations on 25th (first column), 28th (second column) and 31st (third columns) July 2012.



MB ($\mu\text{g}/\text{m}^3$)		O ₃ MDA8				
		<-40	[-40,-10]	[-10,10]	(10,40]	> 40
O ₃ HL	<-40	0	0	0	0	0
	[-40,-10]	0	7 (2%)	0	0	0
	[-10,10]	0	A 35 (10%)	B 94 (28%)	5 (2%)	0
	(10,40]	0	3 (1%)	C 65 (19%)	D 122 (36%)	5 (2%)
	>40	0	0	0	1 (<1%)	5 (2%)

1 - CIP - D 3 - NEIP - B 5 - GV - D 7 - NWIP - D
2 - CIP - B 4 - NEIP - B 6 - GV - D 8 - NWIP - B

5 Figure 5: Air quality stations classified by both mean bias (MB, in $\mu\text{g}/\text{m}^3$) for average hourly and MDA8 O_3 at the Spanish EIONET stations and lumped by categories (A, B, C, and D). Numbered black circles indicate stations under study in Central IP (CIP; station 1 and 2), Northeastern IP (NEIP; station 3 and 4), Guadalquivir Valley (GV; station 5 6), and Northwestern IP (NWIP; station 7 and 8).

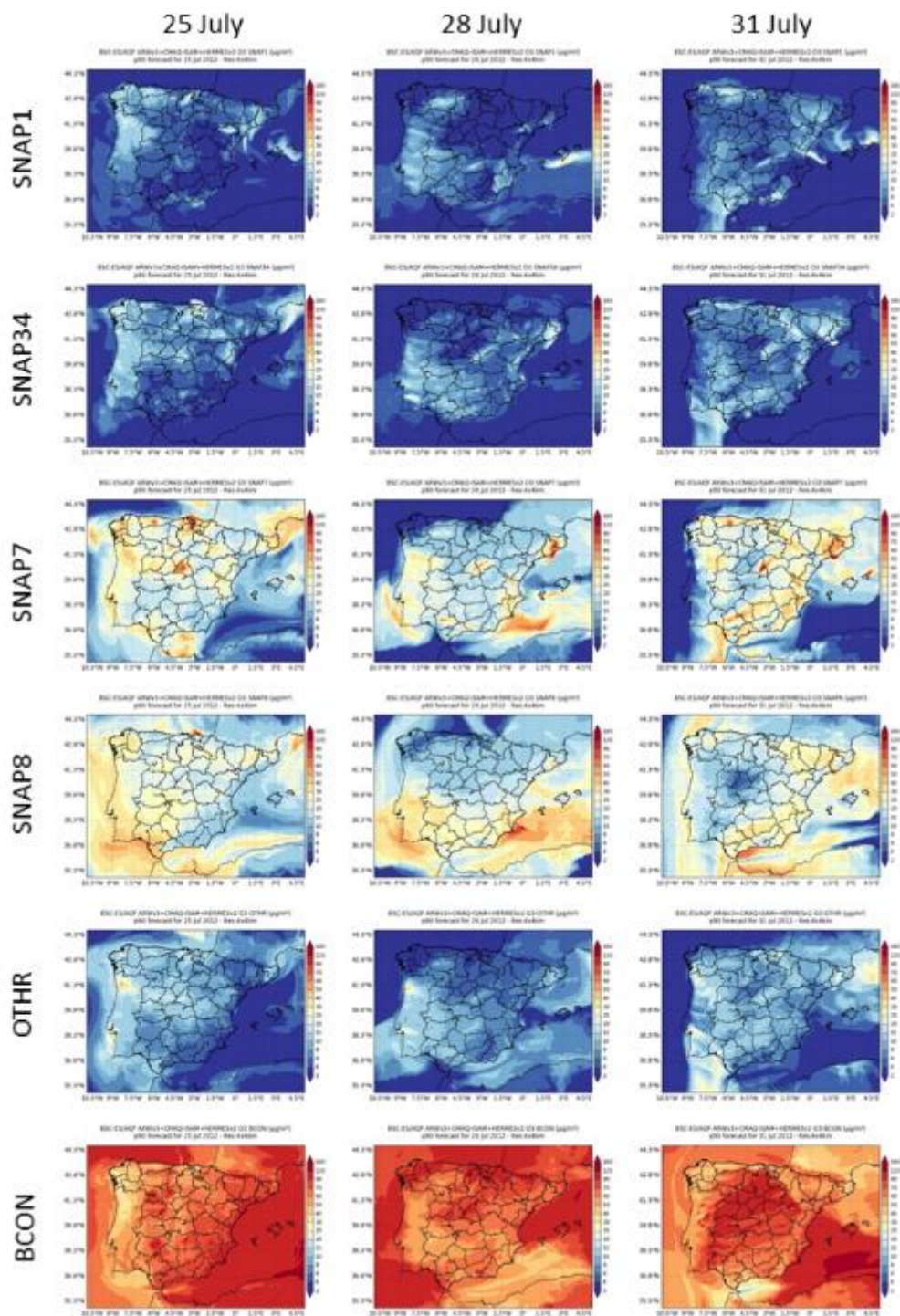


Figure 6: Tagged O_3 concentrations (in μgm^{-3}) corresponding to the 90th percentile (90p) of the average hourly concentrations: SNAP1, SNAP34, SNAP7, SNAP8, OTHER, and BCON for July 25th (first column), 28th (second column) and 31st (third columns) in 2012.

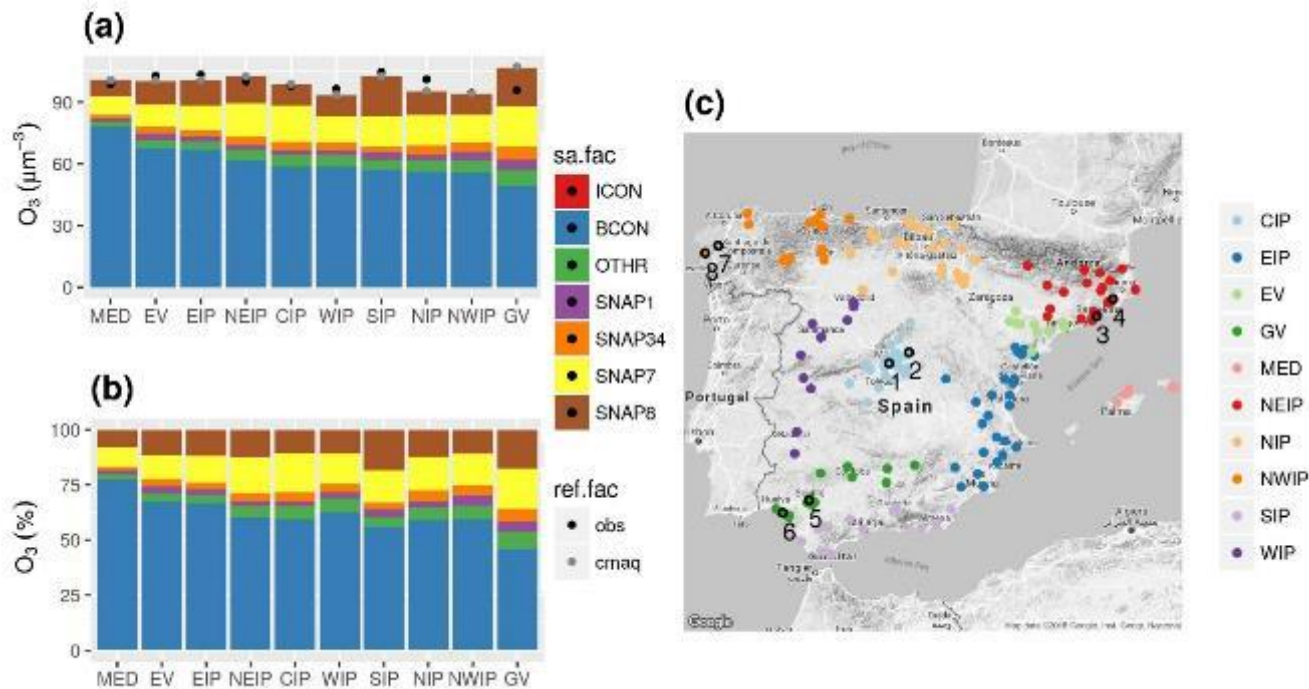


Figure 7: Daily mean contribution in μgm^{-3} (a) and in percentage (b) of tagged sources to O_3 during exceedances of the observed 120 μgm^{-3} for MDA8 O_3 averaged by the identified receptor regions (c). Black and grey dots represent observed and modelled daily mean concentration during exceedances of 120 μgm^{-3} of the observed MDA8 O_3 . Regions correspond to the center of the IP (CIP), the east of the IP (EIP), the Ebro Valley (EV), the Guadalquivir Valley (GV), the Mediterranean Sea (MED), the northeast of the IP (NEIP), the north of the IP (NIP), the northwest of the IP (NWIP), the south of the IP (SIP) and the west of the IP (WIP). Numbered black circles indicate stations under study CI (1-2), NEIP (3-4), GV (5-6) and NWIP (7-8).

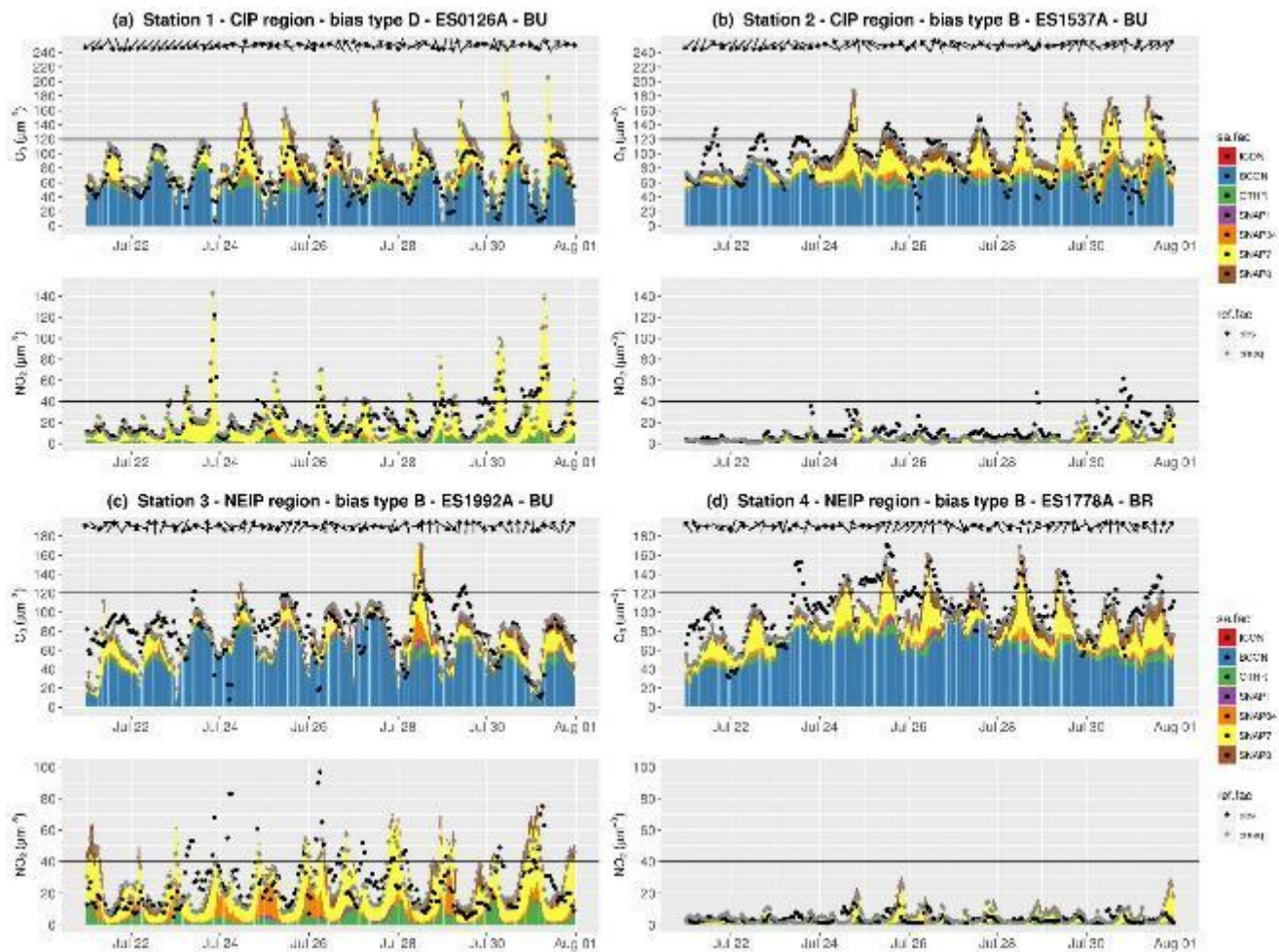


Figure 8: Source apportionment time series for O₃ and NO₂ concentrations (in µgm⁻³) in the episode at the selected stations in the center of the IP (CIP) region (a,b), and in the northeast of the IP (NEIP) (c,d). Color bars (sa.fac) indicate the O₃ tags. Black and grey dots (ref.fac) indicate the observed and modelled concentrations, respectively. Black horizontal lines represent O₃ target value (120 µgm⁻³) and NO₂ limit value (40 µgm⁻³) as a reference. The location of the stations is shown in Fig. 7 by the corresponding numbers.

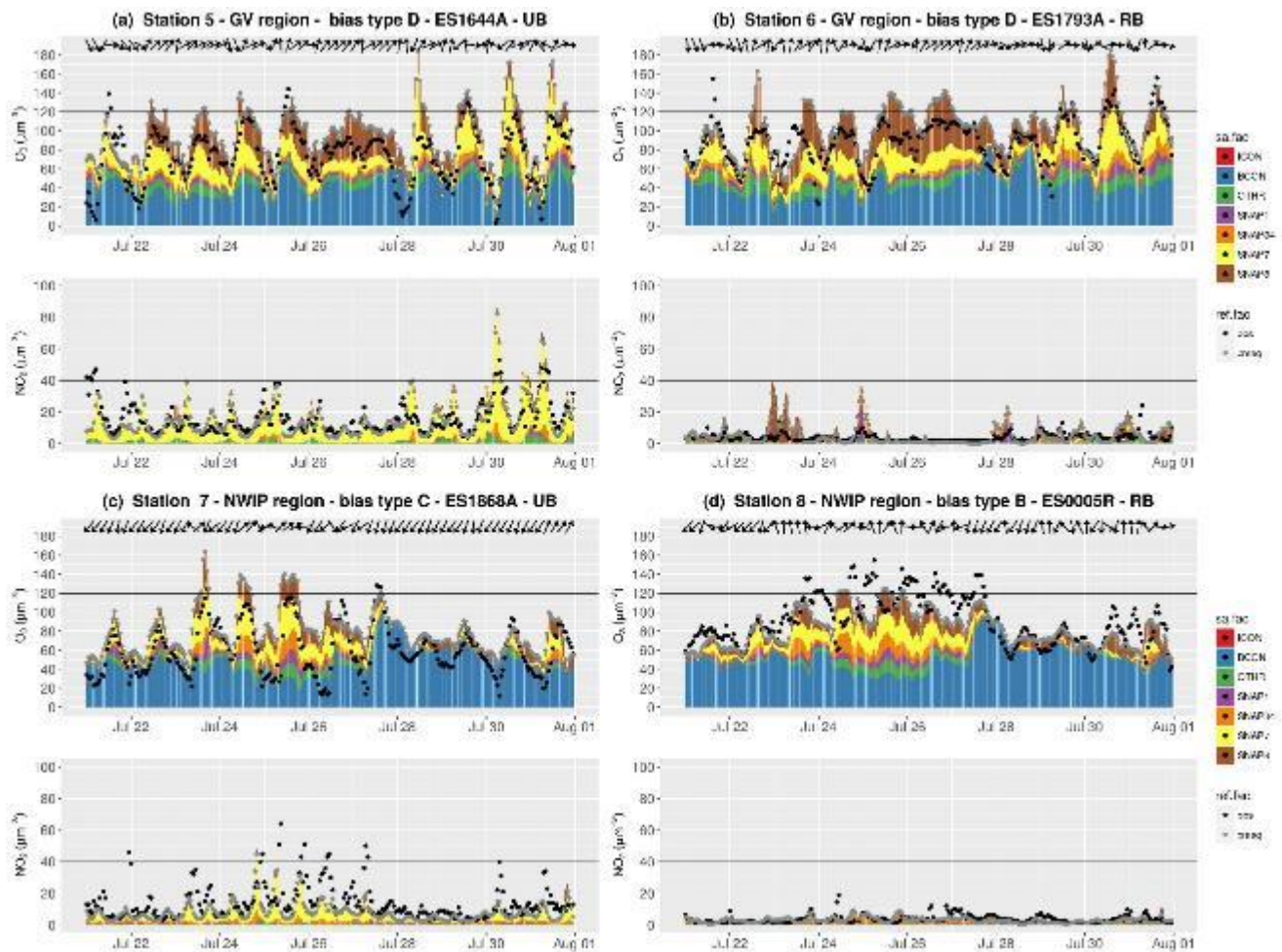


Figure 9: Source apportionment time series for O₃ and NO₂ concentrations (in μgm⁻³) in the episode at the selected stations in the Guadalquivir Valley (GV) (a,b), and in the northwest of the IP (NWIP) (c,d). Color bars (sa.fac) indicate the O₃ tags. Black and grey dots (ref.fac) indicate the observed and modelled concentrations, respectively. Black horizontal lines represent O₃ target value (120 μgm⁻³) and NO₂ limit value (40 μgm⁻³) as a reference. The location of the stations is shown in Fig. 7 by the corresponding numbers.

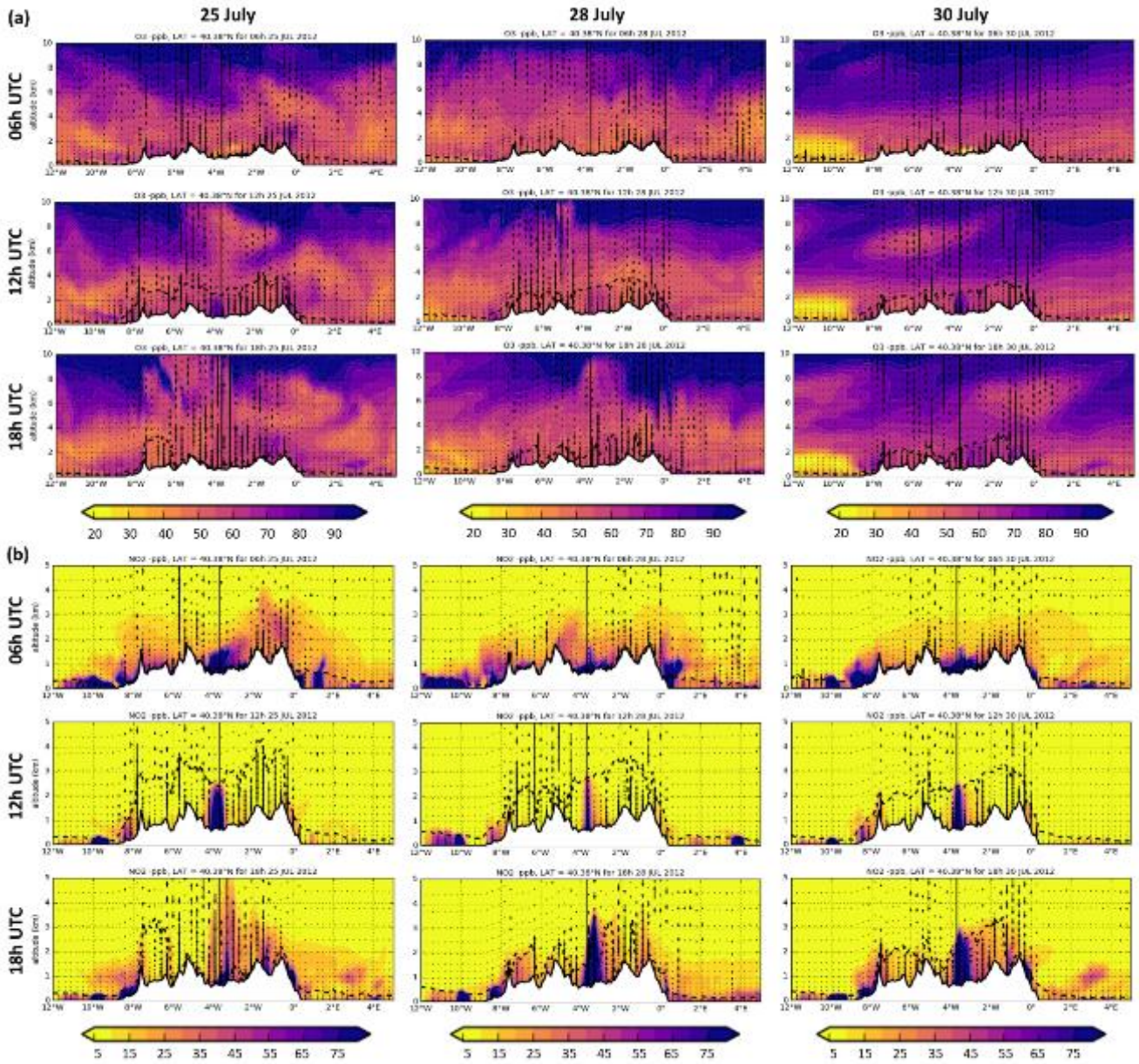


Figure 9: Cross section of modelled mixing ratios (in ppb) for O₃ (a) and NO₂ (b) at a constant latitude (Latitude = 40.38°, Madrid city) of the daily Iberian Thermal Low circulation, equivalent to the conceptual scheme of Millán et al. (1996) for July 25th (first column), 28th (second column) and 30th (third column) at 06, 12 and 18 UTC. Dot lines indicate the boundaries of the planetary boundary layer height. Vertical arrows indicate the vertical wind. Up arrows depict positive winds. Note the different scale for the y-axis between O₃ and NO₂.

Table 1: Description of the O₃ tagged sources in the present study.

ISAM tag*	Emission by SNAP category	Description
SNAP1	SNAP1	SNAP1: Energy industry
SNAP34	SNAP34	SNAP34: Manufacturing industries (combustion and processes)
SNAP7	SNAP7	SNAP7: Road transport, exhaust and non-exhaust
SNAP8	SNAP8	SNAP8: Non-road transport (international shipping, airport and agricultural machinery)
OTHR	SNAP2 + SNAP5 +	SNAP2: residential and commercial/institutional combustion
	SNAP6 + SNAP9 +	SNAP5: Fugitive emissions from fuels
	SNAP10 +	SNAP6: Product use including solvents
	SNAP11	SNAP9: waste management
		SNAP10: Agriculture
		SNAP11: Other sinks
BCON	-	Chemical boundary conditions to IP4 domain from the EU12 simulation which includes the contribution from Europe and international contribution from MOZART-4. O ₃ external contribution
ICON	-	Initial chemical condition of the domain IP4

*Each ISAM tag is applied to O₃ and its precursor species in the CB05 (NO_x and VOCs). NO_x species contributing to O₃ formation involve (9 species): NO, NO₂, nitrogen trioxide (NO₃), dinitrogen pentoxide (N₂O₅), nitrous acid (HONO), peroxyacyl nitrates (PAN), higher peroxyacyl nitrates (PANX), peroxyxynitric acid (PNA), and organic nitrates (NTR). VOC species contributing to O₃ formation include (14 species): acetaldehyde (ALD2), higher aldehydes (ALDX), ethene (ETH), ethane (ETHA), ethanol (ETOH), formaldehyde (FORM), internal olefin (IOLE), isoprene (ISOP), methanol (MEOH), olefin (OLE), paraffin (PAR), monoterpene (TERP), toluene (TOL), and xylene (XYL).

5

10

5

Table 2: Statistics for average hourly O₃, MDA8 O₃, and average hourly NO₂ concentrations in the episode as a function of the station type. Exceedances indicate the number of exceedances of the European Air Quality Directive Standards for hourly O₃ (180 µgm⁻³), MDA8 O₃ (120 µgm⁻³) and average hourly NO₂ (200 µgm⁻³). N indicates the number of monitoring stations used in the statistics calculation. MO and MM depict the measured and modelled mean concentrations, respectively. Statistics are calculated by considering more than 75% of the hours in a day, as established by Directive 2008/50/EC. The statistics correspond to following quantiles 50th (25th, 75th) by station. Type indicates the station categories in the calculation of statistics: all the stations (ALL), industrial (IN), traffic (TR), urban background (UB), suburban background (SB) and rural background (RB) stations.

10

Pollutant	Type	Exceedances: Observed/ Modelled	N	MO (µgm ⁻³)	MM (µgm ⁻³)	MB (µgm ⁻³)	NMB (%)	RMSE (µgm ⁻³)	r
Hourly O ₃	ALL	26/216	348	77.3 (66.7,86.5)	89.9 (83.5,95.6)	12.6 (4.4,20.2)	16.8 (5.1,29.2)	26.7 (21.5,32.1)	0.65 (0.57,0.72)
	IN	5/23	106	74.1 (62.2,83.2)	82.2 (83.4,94.5)	14.1 (4.5,21.5)	19.8 (5.5,34.7)	26.8 (21.1,32.8)	0.66 (0.56,0.73)
	TR	0/58	70	68.4 (57.1,76.7)	83.8 (74.4,89.2)	15.9 (8,21.8)	23.4 (10.1,38.5)	28.8 (24.5,33.9)	0.63 (0.54,0.70)
	UB	0/78	56	74.8 (64.1,80.0)	89.4 (81.4,94.5)	15.6 (7.8,21.3)	22.1 (10.2,31.1)	28.2 (24.5,33.5)	0.65 (0.60,0.70)
	SB	4/48	44	83.2 (78.1,87.2)	93.5 (88.2,97.3)	10 (4.6,14.6)	12.9 (5.4,17.5)	25.1 (21.4,29.3)	0.66 (0.60,0.72)
	RB	17/9	66	91.2 (80.9,97.1)	96.2 (92.6,99.6)	4.5 (-3.3,14.7)	4.8 (-3.2,17.2)	21.2 (18.3,28.0)	0.67 (0.57,0.74)
	MDA8 O ₃	751/822	348	101 (91.0,113.4)	106.2 (101.8,113.2)	5.7 (-3.7,16.9)	5.5 (-3.3,17.4)	17.9 (13.5,25.4)	0.64 (0.39,0.78)
Hourly NO ₂	IN	204/187	106	96.7 (88.9,109.5)	104.8 (99.4,109.2)	5.7 (-2.9,16.5)	5.7 (-2.9,17.8)	17.0 (13.0,24.5)	0.68 (0.48,0.82)
	TR	62/145	70	92.7 (83.6,99.9)	104.1 (98.3,110.2)	13.3 (4.6,23.8)	15.1 (4.6,27.2)	21.2 (15.2,31.2)	0.54 (0.27,0.76)
	UB	86/174	56	100.0 (89.3,105.5)	107.6 (102.2,122.8)	14.1 (2.1,21.7)	14.8 (2.1,22.5)	22.6 (15.6,28)	0.59 (0.34,0.77)
	SB	139/131	44	110.7 (99.8,118.5)	110.0 (105.5,119.2)	3.1 (-6.2,10.5)	2.9 (-5.4,10.1)	16.9 (13.6,22)	0.5 (0.31,0.67)
	RB	260/185	66	113.1 (104.9,119.9)	108.6 (104.5,113.2)	-3.7 (-11.1,5.5)	-3.3 (-9.1,5.1)	15 (11.8,20.2)	0.72 (0.60,0.84)
	ALL	3/0	358	14.0 (8.4,21.2)	9.9 (4.4,16.2)	-4.1 (-8.4,-0.5)	-31.9 (-54.2,-4.9)	12.8 (8.2,17.6)	0.43 (0.29,0.55)
	IN	0/0	120	11.5 (7.9,16.3)	8.8 (3.8,14.7)	-3.0 (-6.6,0.2)	-28.6 (-55.0,1.1)	11.0 (7.9,15.6)	0.40 (0.26,0.50)
	TR	3/0	95	22.9 (17.7,28.7)	14.1 (8.7,21.6)	-7.4 (-13.9,-2.6)	-35.2 (-58.1,-14.3)	18.4 (14.1,23.1)	0.42 (0.28,0.57)
	UB	0/0	63	17.0 (13,21.2)	13.2 (7.8,18.4)	-4.0 (-8,-0.3)	-26.9 (-47.4,-2)	14.1 (10.5,17.3)	0.49 (0.36,0.63)
	SB	0/0	33	12 (8.2,14.6)	7.6 (4.8,11.1)	-2.8 (-6.5,0.8)	-34.4 (-48.6,7.5)	6.4 (7.9,13.6)	0.5 (0.41,0.65)
	RB	0/0	41	4.3 (3.5,9.3)	2.8 (1.6,4.0)	-2.0 (-5.3,-0.3)	-49.5 (-72.3,-9.7)	4.4 (2.7,7.1)	0.34 (0.24,0.43)